Modeling hypoxia-related inflammation scenarios

Mathematical Biosciences 355 (2023) 108952

Contents lists available at ScienceDirect

Mathematical Biosciences

journal homepage: www.elsevier.com/locate/mbs

Original Research Article

Modeling hypoxia-related inflammation scenarios

P. Ferrante [a,b], L. Preziosi [a,*], M. Scianna [a]

[a] Department Mathematical Sciences, Politecnico di Torino, Corso Duca degli Abruzzi 24, Torino, Italy
[b] Candiolo Cancer Institute FPO-IRCCS, Candiolo, Italy

ARTICLE INFO

MSC:
92C37
92C40
92C42
70K50

Keywords:
Hypoxia
Inflammation
Modeling
Stability

ABSTRACT

Cells respond to hypoxia via the activation of three isoforms of Hypoxia Inducible Factors (HIFs), that are characterized by different activation times. HIF overexpression has many effects on cell behavior, such as change in metabolism, promotion of angiogenic processes and elicitation of a pro-inflammatory response. These effects are driving forces of malignant progression in cancer cells. In this work we study in detail hypoxia-induced dynamics of HIF1α and HIF2α, which are the most studied isoforms, comparing available experimental data on their evolution in tumor cells with the results obtained integrating the deduced mathematical model. Then, we examine the possible scenarios that characterize the link between hypoxia and inflammation via the activation of NFkB (Nuclear Factor k-light-chain-enhancer of activated B cells) when the dimensionless groups of parameters of the mathematical model change. In this way we are able to discuss why and when hypoxic conditions lead to acute or chronic inflammatory states.

1. Introduction

Solid tumor microenvironments are typically hypoxic as a result of both an increased demand due to an excessive proliferative rate and a pathological vasculature that is not so effective in oxygen delivery. Hypoxia may differ in duration and extent. As discussed in [1], it can represent a transient condition, that lasts from few minutes to few hours and can be easily reversed; it can be chronic, mainly in the deepest regions of an avascular tumor, i.e., it can persist over a longer period of time (more than one day). It can possibly be cyclic or intermittent, as a consequence of partial and temporal drops in oxygen delivery to the malignant mass from the pre-existing vasculature.

Despite differences in timing and underlying causes, all hypoxic conditions converge through different extents in the activation of one or more HIF isoforms. These are a family of transcription factors, that orchestrate downstream crucial adaptive responses that favor cancer cell survival [2].

They consist of an α subunit, which is regulated in an oxygen dependent manner, and a β subunit, which is constitutively produced. The enzymatic regulation on HIFα is played by a class of prolyl-hydroxylases, PHDs (prolyl hydroxylase domain proteins), that, under normoxic conditions, allow the degradation of HIFα. On the contrary, under hypoxic conditions, HIFα dimerizes with β subunit in order to regulate gene transcription.

Three HIFα isoforms are known, HIF1α, HIF2α, and HIF3α. However, in this article we will focus on the two best characterized isoforms, namely HIF1α and HIF2α, because little about HIF3α from the quantitative point of view. Although HIF1α and HIF2α share similar domain structure, they are characterized by differences in temporal regulation, gene specificity, and tissue expression [3]. Actually, the temporal evolution of HIF1α is very characteristic, presenting a peak of overexpression after a couple of hours from the onset of hypoxia and the tendency to go to a steady state that is characterized by a higher concentration of HIF1α than the normoxic one and is reached within few more hours [4]. HIF2α behaves similarly, but the time scales characterizing the process are one order of magnitude higher [5]. So, it is activated if hypoxia persists for longer periods.

HIFs regulate the expression of more than one thousand target genes encoding proteins involved in hypoxic responses [6]. Among them, we will focus on their influence on alarmin receptors which result overexpressed in hypoxic conditions [7]. The binding of alarmins, released by necrotic cells present in the environment, to their receptors generates a signaling cascade that ends with the activation of NFkB. This, in turn, increases the expression of alarmin receptors triggering an inflammatory state [8–10]. Even if inflammation can either precede or accompany tumor development, in most of the cases it is promoted by the tumor microenvironment ("tumor-elicited inflammation") [11]. In this latter case, inflammation feed into a feed-forward loop of inflammation-induced signaling and becomes non-resolving, leading to a chronic response that lasts for prolonged periods beyond the stimulus that initially triggered it [8].

From the modeling point of view, several papers focused on a detailed dynamics of HIF1, which is the most studied isoform. In particular, in [4,12] a simple kinetic model including HIF1 and three PHD

* Corresponding author.
E-mail addresses: patrizia.ferrante@unito.it (P. Ferrante), luigi.preziosi@polito.it (L. Preziosi), marco.scianna@polito.it (M. Scianna).

https://doi.org/10.1016/j.mbs.2022.108952
Received 15 May 2022; Received in revised form 26 November 2022; Accepted 1 December 2022
Available online 14 December 2022

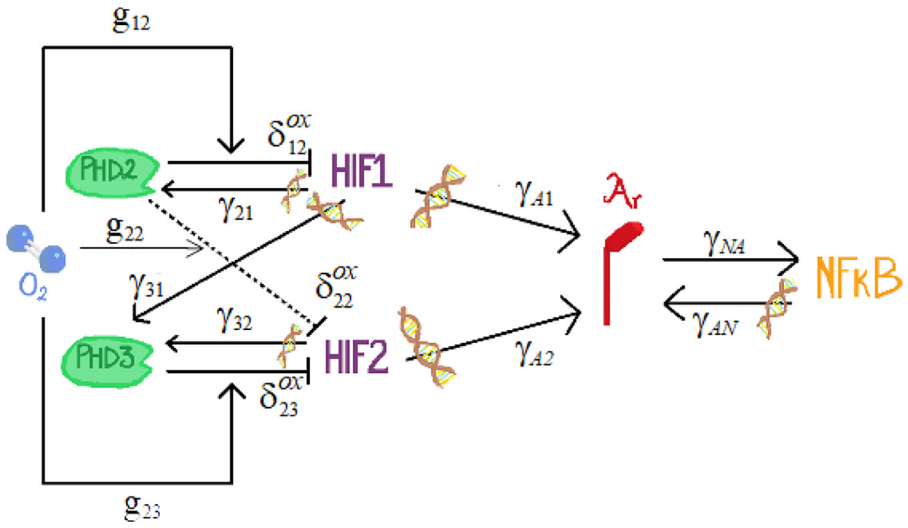

Fig. 1. HIF-PHD-NFkB pathway. Arrows refer to promoting actions, while blockhead arrows to inhibitory actions. The fact that HIF2 degradation is regulated by PHD3 and to a minor extent by PHD2 is described respectively by a full and a dashed blockhead arrow. Basal productions and degradations are not reported for sake of simplicity. DNA schemes refer to the transcriptional activity of HIFs and NFkB.

isoforms is able to reproduce, by suitably fitting the model parameters cell by cell, the outcomes of experiments performed on HeLa cells by the same authors, including the above-mentioned peak dynamics. A more detailed model taking into account both the transcriptional activity of HIF1 and its regulation by both PHD2 and the asparaginyl hydroxylase FIH (Factor Inhibiting HIF) is proposed by Nguyen et al. [13], as well as by Yu et al. [14], who however deal with a generic HIF and PHD. The main focus of these works is to describe how the variables at equilibrium depend from the oxygen concentration. Less attention is payed to whether the models are able to catch the peak dynamics. Other models dealing with the regulation of HIF1 by PHD2 are proposed in [15–17].

The description of the relationship between HIF1 dynamics and aerobic/anaerobic energy metabolism is the aim of the model proposed in [18]. The mathematical model consists in 16 ODEs with a particular focus on the dynamics of the metabolism-related proteins in the cytoplasm and in the mitochondria. With the same aim, Kelly et al. [19] propose a simpler model consisting of an ODE for the evolution of HIF1 and three reaction–diffusion equations for the spatio-temporal evolution of glucose, oxygen and 18-fluorodeoxyglucose. Their main aim is then to describe how the concentration of the state variables above depends on the distance from a vessel.

Still regarding other consequences of hypoxia, the interaction between HIF and cyclin expression governing the G1/S transition and therefore cell cycle is described in [20,21]. On the other hand, Coulibaly et al. [22] study how the overexpression of interleukines activates downstream a cascade of activations involving AKT-mTOR pathway that leads to the overexpression of HIF1α.

The aim of the present article is to model the interplay between hypoxic state and inflammatory response from a different point of view. In fact, since alarmin receptors can be a potential target of both HIF1 and HIF2 [23], we investigate the role of both HIF1 and HIF2 overexpression as well as the role of their regulators PHD2 and PHD3 on the activation of an inflammatory response. Moreover, we will not describe the details of the dimerization process and of HIF transfection to the nucleus, which was for instance the focus of the work by Nguyen et al. [13], and will only focus on HIFα that represents the rate limiting factor for HIF dimerization.

Specifically, in Section 2 we deduce the mathematical model of the HIF-PHD-NFkB pathway and in Section 3 we discuss the stability character of the equilibrium states. Then, we first study in detail the dynamics of HIF1 (Section 4.1) and HIF2 (Section 4.2) comparing them with available experimental data on their evolution as well as on that of PHD2. Then, in the lack of quantitative data on NFkB evolution directly linked to HIFs, in Section 5 we examine the possible scenarios that might characterize the link between hypoxia and inflammation as a function of the dimensionless groups of parameters characterizing the mathematical model. In this way, we are able to discuss when hypoxic conditions lead to acute or chronic inflammatory states, distinguish between the cases in which the chronic inflammation is self-sustaining and explore strategies that may lead to the resolution of the inflammation. For instance, we show that if the transcriptional activity of NFkB on genes that encode for alarmin receptors is sufficiently high, then the inflammatory state, if triggered, is irreversible, even if normoxic conditions are re-established. In this case a way (the only way) to resolve inflammation would be to pharmacologically target NFkB activation impacting either directly or indirectly on its transcriptional activity.

2. Mathematical model of the HIF-PHD-NFkB pathway

The response of cells as a function of oxygen availability is regulated by the activity of HIFs that are in turn regulated by PHDs. As mentioned in the Introduction, in presence of oxygen, PHDs hydroxylate HIFα subunit on two proline residues targeting it for proteasomal degradation [2]. On the contrary, under hypoxic conditions PHDs display little catalytic activity, so that HIFs remain unhydroxylated and therefore stabilized becoming overexpressed and transcriptionally active. Referring to Fig. 1, HIF1 and HIF2 are related to specific PHDs, named respectively PHD2 [24] and PHD3 [25], though it is found that PHD2 has a minor regulatory activity on HIF2 [25]. In particular, HIF1 promotes both PHD2 and PHD3 production [24–26], whereas HIF2 promotes PHD3 production only [25].

Coming to the inflammatory part, the stabilization of both HIFs in tumor cells induces the expression of alarmin receptors on their plasma membrane [7]. These receptors, once bound to alarmins released by tumor-associated necrosis, generate a signaling cascade that ends with the activation of NFkB, which in turn contributes to the expression of alarmin receptors, thus forming a positive feedback loop. NFkB activation then leads to a cell inflammatory state [8–10].

With the aim of describing the evolution of the pathway above in response to oxygen availability, in the following we will denote with $\hat{H}_1$ and $\hat{H}_2$ the nuclear level of HIF1 and HIF2 and with $\hat{P}_2$ and $\hat{P}_3$ the cellular level of their main regulators PHD2 and PHD3. Then, the role of alarmin receptors and of NFkB will be respectively described by the variables $\hat{A}_r$ and $\hat{N}$. To clarify the general notation used in the following equations, we explicitly observe that hatted variables

are dimensional as well as hatted functions (e.g., $\hat{\Gamma}_\alpha$ for $\alpha = A, 2, 3$ below), while non-hatted counterparts and functions are dimensionless quantities, including g_{ij} and F_{ij} below.

Oxygen concentration $\hat{O}_2$ is taken as externally controlled, i.e., it is described by a given function of time, which typically has a piecewise constant trend ranging either from *normoxic* to *hypoxic* values or *vice versa* (see the Appendix for the quantitative definition of normoxia and hypoxia that will be used in this paper). In deducing the model, we will focus on the post-translational modification of the proteins played by the PHDs. We skip other types of regulation, such as the transcriptional one, that may contribute to the switch between HIF1 and HIF2, as discussed in [27] in the specific scenario of non-tumor cell lines.

Let us start the model deduction by focusing on HIF1 and HIF2 dynamics. They are basally synthesized at a rate γ_1 and γ_2, respectively, and are degraded in an oxygen-independent way at a rate δ_1 and δ_2. However, referring to Fig. 1, they undergo a more relevant oxygen-dependent degradation: in the case of HIF1, it is triggered by PHD2 at a rate δ_{12}^{ox}, whereas in the case of HIF2, it is triggered by both PHD2 and PHD3 at rates δ_{22}^{ox} and δ_{23}^{ox}, respectively, being $\delta_{23}^{ox} > \delta_{22}^{ox}$ in agreement with experimental evidences reported in [25]. Summing up, the evolution of HIF1 and HIF2 is modeled by the following ODEs

$$\frac{d\hat{H}_1}{d\hat{t}} = \gamma_1 - \delta_1 \hat{H}_1 - \delta_{12}^{ox} g_{12}(\hat{O}_2) F_{12}(\hat{H}_1) \hat{P}_2 , \tag{1}$$

$$\frac{d\hat{H}_2}{d\hat{t}} = \gamma_2 - \delta_2 \hat{H}_2 - \delta_{22}^{ox} g_{22}(\hat{O}_2) F_{22}(\hat{H}_2) \hat{P}_2 - \delta_{23}^{ox} g_{23}(\hat{O}_2) F_{23}(\hat{H}_2) \hat{P}_3 , \tag{2}$$

where

$$g_{ij}(\hat{O}_2) = \frac{\hat{O}_2}{K_{ij}^{ox} + \hat{O}_2} \quad \text{and} \quad F_{ij}(\hat{H}_i) = \frac{\hat{H}_i}{K_{ij} + \hat{H}_i} , \tag{3}$$

are dimensionless Michaelis–Menten terms describing the degradation of HIF1 and HIF2 by PHD2 and PHD3 (as given by the F terms), that is promoted by the presence of oxygen (as given by the g terms). For the sake of clarity, we notice that the double index hk refers to the action on h due to the presence of k. So, for instance, δ_{23}^{ox} refers to the degradation of HIF2 due to the presence of PHD3.

As seen, PHD2 production is triggered by HIF1 whereas PHD3 production by both HIFs. Taking into account also of their natural degradation at rates δ_{P_2} and δ_{P_3}, respectively we can write

$$\frac{d\hat{P}_2}{d\hat{t}} = \gamma_{21} \hat{\Gamma}_2(\hat{H}_1) - \delta_{P_2} \hat{P}_2 , \tag{4}$$

$$\frac{d\hat{P}_3}{d\hat{t}} = \gamma_{32} \hat{\Gamma}_3(\hat{H}_1, \hat{H}_2) - \delta_{P_3} \hat{P}_3 . \tag{5}$$

In the perspective of an analysis of equilibrium configurations and of the corresponding stability characteristics, we assume that the two source functions $\hat{\Gamma}_2(\hat{H}_1)$ and $\hat{\Gamma}_3(\hat{H}_1, \hat{H}_2)$ are increasing in their arguments and vanish when $\hat{H}_1 = \hat{H}_2 = 0$.

Coming to the inflammatory part, in our set-up, we are assuming that alarmins are present in the microenvironment in such a way that the limiting factor for triggering inflammation is represented by the level of expression of their cell receptors only, rather than by the presence of alarmin factors themselves. As already mentioned, the expression of alarmin receptors is induced by both NFkB, at a rate γ_{AN} and through an increasing function of $\hat{N}$, $\hat{G}_A(\hat{N})$, and HIFs, through the function $\hat{\Gamma}_A(\hat{H}_1, \hat{H}_2)$, which has an increasing trend w.r.t. its arguments $\hat{H}_1$ and $\hat{H}_2$, as hypothesized in [28]. Assuming a constant degradation of alarmin receptors at rate δ_A, we can write:

$$\frac{d\hat{A}_r}{d\hat{t}} = \gamma_{A1} \hat{\Gamma}_A(\hat{H}_1, \hat{H}_2) + \gamma_{AN} \hat{G}_A(\hat{N}) - \delta_A \hat{A}_r . \tag{6}$$

Finally, NFkB is assumed to be produced both basally, at a rate γ_N, and through an Hill-type action of $\hat{A}_r$, also on the basis of [29],

$$G_N(\hat{A}_r) = \frac{\hat{A}_r^2}{K_A^2 + \hat{A}_r^2} , \tag{7}$$

and to be degraded at a constant rate δ_N, so that we can write

$$\frac{d\hat{N}}{d\hat{t}} = \gamma_N + \gamma_{NA} G_N(\hat{A}_r) - \delta_N \hat{N} . \tag{8}$$

Despite, as we shall see, the stability analysis is independent from the specific form given to $\hat{\Gamma}_2$, $\hat{\Gamma}_3$, $\hat{\Gamma}_A$, and $\hat{G}_A$, in the forthcoming simulations, we opt for simple linear trends

$$\begin{aligned} &\hat{\Gamma}_2(\hat{H}_1) = \hat{H}_1 , \quad \hat{\Gamma}_3(\hat{H}_1, \hat{H}_2) = \sigma \hat{H}_1 + \hat{H}_2 , \\ &\hat{G}_A(\hat{N}) = \hat{N} , \quad \hat{\Gamma}_A(\hat{H}_1, \hat{H}_2) = \hat{H}_1 + \rho \hat{H}_2 . \end{aligned} \tag{9}$$

So, overall, HIF-PHD-NFkB kinetics are modeled by Eqs. (1), (2), (4), (5), (6), and (8), complemented by (3) and (7). It is however useful to rewrite the system in a non-dimensional form. In this respect, let us introduce the following scaled variables

$$\begin{aligned} &H_1 = \frac{\hat{H}_1}{K_{12}} , \quad H_2 = \frac{\hat{H}_2}{K_{23}} , \quad P_2 = \frac{\delta_{P_2}}{\gamma_{21} K_{12}} \hat{P}_2 , \quad P_3 = \frac{\delta_{P_3}}{\gamma_{32} K_{23}} \hat{P}_3 , \\ &A_r = \frac{\hat{A}_r}{K_A} , \quad N = \frac{\delta_N}{\gamma_{NA}} \hat{N} , \quad O_2 = \frac{\hat{O}_2}{K_{12}^{ox}} , \quad t = \delta_{P_2} \hat{t} . \end{aligned}$$

In addition, we define

$$\Gamma_2 = \frac{\hat{\Gamma}_2}{K_{12}} , \quad \Gamma_3 = \frac{\hat{\Gamma}_3}{K_{23}} , \quad \Gamma_A = \frac{\gamma_{A1} \hat{\Gamma}_A}{\delta_A K_A} , \quad \text{and} \quad G_A = \frac{\gamma_{AN} \hat{G}_A}{\delta_A} .$$

The resulting dimensionless system of equations finally reads as

$$\tau \frac{dH_1}{dt} = 1 - \zeta H_1 - \eta g_{12}(O_2) F_{12}(H_1) P_2 , \tag{10}$$

$$\frac{dP_2}{dt} = \Gamma_2(H_1) - P_2 , \tag{11}$$

$$\tau_2 \frac{dH_2}{dt} = 1 - \zeta_2 H_2 - \eta_2 g_{22}(O_2) F_{22}(H_2) P_2 - \eta_3 g_{23}(O_2) F_{23}(H_2) P_3 , \tag{12}$$

$$\tau_P \frac{dP_3}{dt} = \Gamma_3(H_1, H_2) - P_3 , \tag{13}$$

$$\tau_A \frac{dA_r}{dt} = \Gamma_A(H_1, H_2) + \beta G_A(N) - A_r , \tag{14}$$

$$\tau_N \frac{dN}{dt} = \alpha + G_N(A_r) - N , \tag{15}$$

with

$$\begin{aligned} &\tau = \frac{K_{12} \delta_{P_2}}{\gamma_1} , \quad \zeta = \frac{K_{12} \delta_1}{\gamma_1} , \quad \eta = \frac{K_{12} \gamma_{21} \delta_{12}^{ox}}{\gamma_1 \delta_{P_2}} , \\ &\tau_2 = \frac{K_{23} \delta_{P_2}}{\gamma_2} , \quad \zeta_2 = \frac{K_{23} \delta_2}{\gamma_2} , \quad \eta_2 = \frac{K_{12} \gamma_{21} \delta_{22}^{ox}}{\gamma_2 \delta_{P_2}} , \quad \eta_3 = \frac{K_{23} \gamma_{32} \delta_{23}^{ox}}{\gamma_2 \delta_{P_3}} , \\ &\tau_P = \frac{\delta_{P_2}}{\delta_{P_3}} , \quad \tau_A = \frac{\delta_{P_2}}{\delta_A} , \quad \tau_N = \frac{\delta_{P_2}}{\delta_N} , \quad \alpha = \frac{\gamma_N}{\gamma_{NA}} , \\ &\beta = \frac{\gamma_{AN} \gamma_{NA}}{\delta_A \delta_N K_A} . \end{aligned}$$

For sake of completeness we also mention that F_{ij}, g_{ij}, and G_N are now written as functions of dimensionless quantities with suitably scaled Michaelis–Menten constants, i.e.,

$$\begin{aligned} &g_{12}(O_2) = \frac{O_2}{1 + O_2} , \quad g_{22}(O_2) = \frac{O_2}{\tilde{K}_{22}^{ox} + O_2} , \quad g_{23}(O_2) = \frac{O_2}{\tilde{K}_{23}^{ox} + O_2} , \\ &F_{12}(H_1) = \frac{H_1}{1 + H_1} , \quad F_{22}(H_2) = \frac{H_2}{\tilde{K}_{22} + H_2} , \quad F_{23}(H_2) = \frac{H_2}{1 + H_2} , \\ &G_N(A_r) = \frac{A_r^2}{1 + A_r^2} , \end{aligned}$$

where $\tilde{K}_{22}^{ox} = K_{22}^{ox}/K_{12}^{ox}$, $\tilde{K}_{23}^{ox} = K_{23}^{ox}/K_{12}^{ox}$, and $\tilde{K}_{22} = K_{22}/K_{23}$.

Referring to the Appendix for a discussion on the evaluation of the model parameters, in Table 1 we list the reference values related to the HIF-PHD dynamics. Then, in Section 4.1.2 we will describe the influence of parameter changes on HIF dynamics.

3. Equilibrium and stability

In this section we will show how, for any given oxygen concentration, it is possible to identify the equilibrium states examining in

Table 1
Parameters used as reference values for the HIF-PHD dynamics in Eqs. (1)–(8) and related dimensionless parameters in Eqs. (10)–(15). A discussion of how they have been estimated is contained in the Appendix. The acronym "M-M" stands for Michaelis–Menten.

Reference values of model parameters					
Parameter (unit)	HIF1		HIF2	PHD2	PHD3
Basal production (μM/s)	$\gamma_1 = 10^{-1}$		$\gamma_2 = 3 \cdot 10^{-1}$		
Basal degradation (s^{-1})	$\delta_1 = 10^{-5}$ [4,13]		$\delta_2 = 10^{-5}$	$\delta_{P_2} = 10^{-5}$ [4,13]	$\delta_{P_3} = 10^{-5}$
Parameter (unit)	HIF1 → PHD2		HIF1 → PHD3		HIF2 → PHD3
PHD production (s^{-1})	$\gamma_{21} = 4 \cdot 10^{-5}$ [12]		$\gamma_{31} = 4 \cdot 10^{-5}$		$\gamma_{32} = 2 \cdot 10^{-5}$
	HIF1 ← PHD2		HIF2 ← PHD2		HIF2 ← PHD3
HIF degradation by PHD (s^{-1})	$\delta_{12}^{ox} = 10^{-2}$ [30,31]		$\delta_{22}^{ox} = 7 \cdot 10^{-3}$ [30]		$\delta_{23}^{ox} = 10^{-4}$
M-M constant (O_2) (μM)	$K_{12}^{ox} = 100$ [30,32,33]		$K_{22}^{ox} = 70$ [34]		$K_{23}^{ox} = 100$
M-M constant (HIF) (μM)	$K_{12} = 14$ [30,31]		$K_{22} = 15$ [34]		$K_{23} = 150$ [32]
Reference values of dimensionless model parameters					
$\eta = 5.6$	$\eta_2 = 1.3067$	$\eta_3 = 0.1$	$\tau = 1.4 \cdot 10^{-3}$	$\tau_2 = 5 \cdot 10^{-2}$	$\tau_P = 1$
$\zeta = 1.4 \cdot 10^{-3}$	$\zeta_2 = 5 \cdot 10^{-2}$	$\sigma = 0.19$	$\tilde{K}_{22}^{ox} = 0.7$	$\tilde{K}_{23}^{ox} = 1$	$\tilde{K}_{22} = 0.1$

cascade the subsystem formed by Eqs. (10)–(11), i.e., relative to HIF1 and PHD2 kinetics, to pass then to Eqs. (12)–(13), i.e., relative to HIF2 and PHD3 kinetics, to end with Eqs. (14)–(15), i.e., relative to alarmin receptors and NFkB kinetics. Subsequently, the stability character of the equilibria will be discussed under the following biologically funded hypothesis.

Hyp1: The functions $\Gamma_2(H_1)$, $\Gamma_3(H_1, H_2)$, $\Gamma_A(H_1, H_2)$, and $G_A(N)$ of the dimensionless system (10)–(15) are increasing from zero in their arguments, i.e.,

$$\Gamma_2(0) = \Gamma_3(0,0) = \Gamma_A(0,0) = 0\,, \quad \text{and}$$

$$\frac{\partial \Gamma_2}{\partial H_1}(H_1) > 0\,, \quad \frac{\partial \Gamma_3}{\partial H_1}(H_1, H_2) > 0\,, \quad \frac{\partial \Gamma_3}{\partial H_2}(H_1, H_2) > 0,$$

$$\frac{\partial G_A}{\partial N}(N) > 0\,, \quad \frac{\partial \Gamma_A}{\partial H_1}(H_1, H_2) > 0\,, \quad \frac{\partial \Gamma_A}{\partial H_2}(H_1, H_2) > 0,$$

$\forall H_1, H_2, N.$

3.1. Equilibrium states

We start by noticing that, from Eq. (11), $P_2^{eq} = \Gamma_2(H_1^{eq})$, which, substituted in (10) allows to get

$$\zeta H_1^{eq} + \eta g_{12}(O_2) F_{12}(H_1^{eq}) \Gamma_2(H_1^{eq}) = 1\,, \tag{16}$$

and therefore to implicitly identify H_1^{eq}. Because of the positivity requirement and of the increasing trend of the functions Γ_2 and F_{12} and of the fact that $\Gamma_2(H_1 = 0) = 0$, Eq. (16) has only one solution. Actually, since the term g_{12} increases with the concentration of oxygen, the derivative of the l.h.s. of (16) at any fixed H_1 increases with O_2 as well, and then we can also state that both H_1^{eq} and P_2^{eq} decrease with the level of available oxygen, as expected and shown in Fig. 2a,b,c.

Specifically, if $\Gamma_2(H_1) = H_1$ we can explicitly write

$$H_1^{eq} = P_2^{eq} = \frac{1 - \zeta + \sqrt{(1+\zeta)^2 + 4\eta g_{12}(O_2)}}{2[\zeta + \eta g_{12}(O_2)]}\,. \tag{17}$$

The dependence of this equilibrium value from the dimensionless parameters is reported in Fig. 2a,b,c. The estimated value of ζ reported in Table 1 is much smaller than 1, so that in (17), the ζ terms could be even dropped. In fact, looking at Fig. 2b, in order to see a valuable difference in the dependence of the equilibrium concentration of HIF1 from the oxygen level, ζ has to increase up to biologically unrealistic values close to 0.1, as expected. The presence of ζ becomes relevant for extremely low concentrations of oxygen. In particular, the curve goes to $1/\zeta$ when the oxygen level drops to zero.

Fig. 2a instead describes how H_1^{eq}, and therefore P_2^{eq}, decrease for increasing concentrations of O_2 for different values of the parameter η. Fig. 2c finally compares the experimental values of HIF1 reported in [35] for HeLa cells and the equilibrium values obtained by the model for the reference values $\eta = \eta_0 = 5.6$ and $\zeta = \zeta_0 = 1.4 \cdot 10^{-3}$. We observe that, in [35] and in Fig. 2c, HIF1 levels are normalized with respect to the value obtained for a saturation of oxygen of 6% corresponding to a non-dimensional $O_2 = 0.6$.

For sake of clarity, we need to distinguish between PHD2 and the enzymatically active PHD2. In fact, Fig. 2d shows the level of enzymatically active PHD2 (denoted by P_2^*), that corresponds to multiplying P_2 by the Michaelis–Menten term g_{12}, and its increasing dependence from the oxygen level. This behavior is in agreement with published experimental evidence [30] and shows a steep decrease going back toward anoxic conditions $O_2 \ll 0.1$.

Proceeding in a similar way for HIF2, Eq. (13) readily gives $P_3^{eq} = \Gamma_3(H_1^{eq}, H_2^{eq})$, where now H_1^{eq} can be considered known from Eq. (17), or from the solution of Eq. (16). Substituting P_3^{eq} and P_2^{eq} in (12) we can write

$$\zeta_2 H_2^{eq} + \eta_2 g_{22}(O_2) F_{22}(H_2^{eq}) \Gamma_2(H_1^{eq}) + \eta_3 g_{23}(O_2) F_{23}(H_2^{eq}) \Gamma_3(H_1^{eq}, H_2^{eq}) = 1\,, \tag{18}$$

that allows to implicitly determine H_2^{eq}. In particular, the above-mentioned properties of F_{22}, F_{23}, Γ_2 and Γ_3 (see Hyp1) result in the existence of a single equilibrium state, H_2^{eq}, that, as expected, decreases with the level of oxygen. The same holds for P_3^{eq}.

We can finally focus on the last two equations. From (15) we have

$$N^{eq} = \alpha + G_N(A_r^{eq})\,, \tag{19}$$

that can be substituted back in (14), to get an implicit equation in A_r^{eq}. Instead of solving the resulting equation in terms of A_r, the presence of the Hill form of G_N defined in (7), as well as the still undefined function G_A, suggests to rewrite it as

$$\Gamma_A(H_1^{eq}, H_2^{eq}) = A_r^{eq} - \beta G_A\left(\alpha + G_N(A_r^{eq})\right). \tag{20}$$

Considering that H_1^{eq} and H_2^{eq} are decreasing functions of the given and controlled oxygen level O_2, we can look for the number of solutions of (21) as a function of the oxygen level, or, equivalently, of Γ_A. However, in order to clarify the discussion, we take the specific form of $G_A(N) = N$, so that (20) simplifies in

$$\Gamma_A(H_1^{eq}, H_2^{eq}) = A_r^{eq} - \beta\left(\alpha + G_N(A_r^{eq})\right). \tag{21}$$

Now, as can be trivially checked, G_N is always increasing with derivative that, starting from zero, increases up to $G'_{N,max} = \frac{3\sqrt{3}}{8}$ to

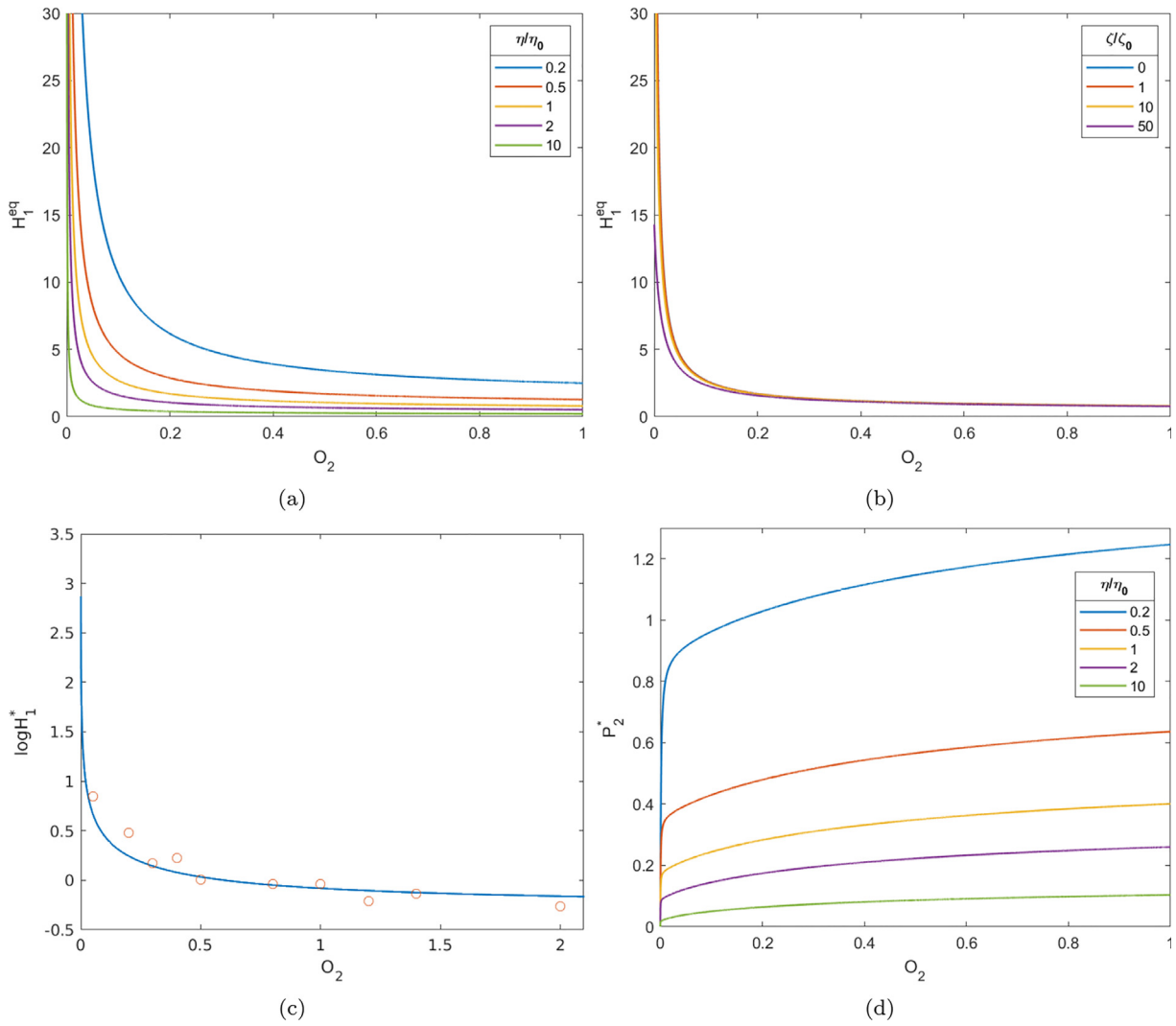

Fig. 2. Dependence of non-dimensional HIF1 and PHD2 levels plotted as a function of O_2 normalized with respect to K_{12}. For reference, $O_2 = 1$ corresponds to a saturation of 10% and then to normoxic conditions in tissues. In the top row HIF1-level at equilibrium for different values of the dimensionless parameters η (a) and ζ (b). Specifically, top to bottom in (a) $\eta/\eta_0 = 0.2, 0.5, 1, 2, 10$ and in (b) $\zeta/\zeta_0 = 0, 1, 10, 50$ where the reference values $\eta_0 = 5.6$ and $\zeta_0 = 1.4 \cdot 10^{-3}$ are based on data reported in Table 1. In (b) the results for the first three values almost overlap. (c) Comparison between numerical (blue line) and experimental (red circles) HIF1 equilibrium values in HeLa cells normalized with respect to the value obtained at 6% O_2 as a function of the oxygen level (normalized with respect to $K_{12} = 100\,\mu M$), i.e., $H^*(O_2) = H_1^{eq}(O_2)/H_1^{eq}(O_2 = 0.6)$, as reported in [35]. The line corresponds to the equilibrium values predicted by the model in the reference case $\eta = \eta_0$ and $\zeta = \zeta_0$. (d) Level of enzymatically active PHD2 ($P_2^*(O_2) = g(O_2)P_2^{eq}(O_2)$) at equilibrium, taking into account the Michaelis–Menten term in Eq. (3), for increasing values of η/η_0 from top to bottom.

decrease again to zero. So, if

$$G'_{N,max} = \frac{3\sqrt{3}}{8} < \frac{1}{\beta}, \tag{22}$$

then the r.h.s. of (21) is always increasing (starting from a non biological negative value when $A_r > 0$) and so there is a only one equilibrium state. Otherwise, if $\frac{1}{\beta} < \frac{3\sqrt{3}}{8}$ there are two values of A_r for which the derivative of the r.h.s. vanishes. So, there might be three admissible equilibria, suggesting the existence of a saddle–node bifurcation, as it will be discussed in the following section.

The bistability range can be identified looking for the points where the curve given by (21) is tangent to the A_r axis either at its minimum or at its maximum. These points can be identified solving the system

$$\begin{aligned} &A_r - \beta\left(\alpha + \frac{A_r^2}{1+A_r^2}\right) = 0 \\ &1 - \beta\frac{2A_r}{(1+A_r^2)^2} = 0\,. \end{aligned} \tag{23}$$

In the (α, β) plane the system above identifies the curve

$$\begin{cases} \alpha = \dfrac{A_r^2(1-A_r^2)}{(1+A_r^2)^2} \\ \beta = \dfrac{(1+A_r^2)^2}{2A_r} \end{cases} \tag{24}$$

for $A_r \in (0, 1]$, being α non negative. The curve presents a cusp in $\alpha = \frac{1}{8}$ and $\beta = \frac{8}{9}\sqrt{3}$. Then, as shown in Fig. 3a, the parameter plane is divided in 4 zones:

- in I, there is only one equilibrium (as the rightmost curve in Fig. 3b,c);
- in II, there are three equilibria in a certain interval of Γ_A and one outside it (as the third full curve in Fig. 3b,c);
- in III, there are three equilibria below a certain value of Γ_A and one above it (as the first two curves in Fig. 3b,c);
- in IV, there is only one admissible equilibrium.

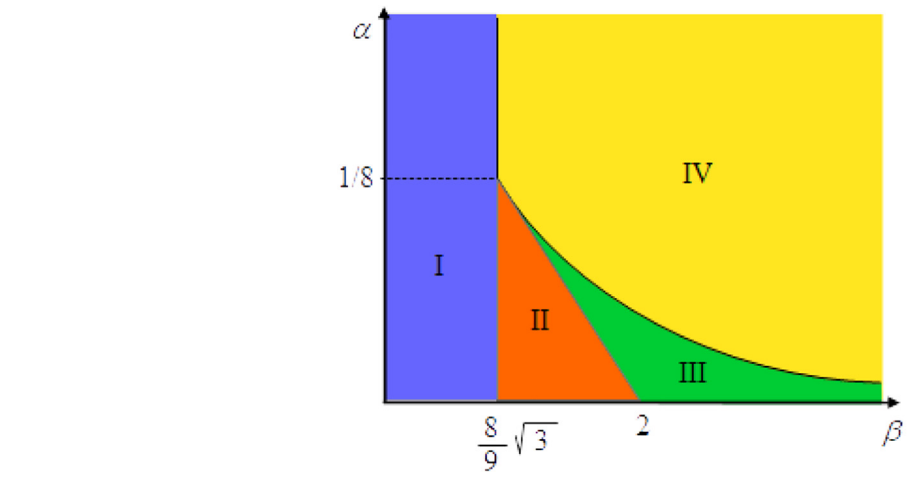

(a)

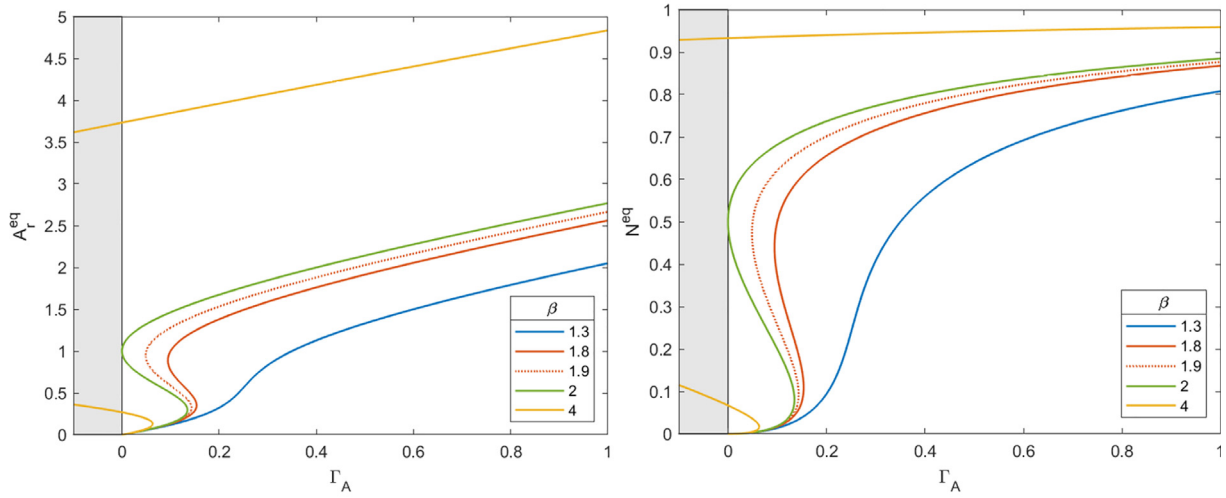

(b) (c)

Fig. 3. (a) Stability regions in the (α, β) plane. (b-c) For each stability region, we plot (in the same color) an example of equilibrium concentrations of alarmin receptors (b) and NFkB (c) as functions of $\Gamma_A(H_1^{eq}(O_2), H_2^{eq}(O_2))$. Specifically, full lines from right to left correspond to zones I up to III with $\beta = 1.3, 1.8, 2, 4$ and $\alpha = 0$ always. The dotted curves correspond to the value $\beta = 1.9$, which will be used in the simulations proposed in Section 5. The shaded gray areas in (b) and (c) correspond to non physiological values of Γ_A.

3.2. Stability

In order to discuss the stability characteristics of the equilibria, we observe that the Jacobian of the system (10)–(15) is

$$J = \begin{pmatrix} -\zeta - \eta g_{12} \dfrac{\partial F_{12}}{\partial H_1} P_2 & -\eta g_{12} F_{12} & 0 & 0 & 0 & 0 \\ \dfrac{\partial \Gamma_2}{\partial H_1} & -1 & 0 & 0 & 0 & 0 \\ 0 & -\eta_2 g_{22} F_{22} & J_{33} & -\eta_3 g_{23} F_{23} & 0 & 0 \\ \dfrac{\partial \Gamma_3}{\partial H_1} & 0 & \dfrac{\partial \Gamma_3}{\partial H_2} & -1 & 0 & 0 \\ \dfrac{\partial \Gamma_A}{\partial H_1} & 0 & \dfrac{\partial \Gamma_A}{\partial H_2} & 0 & -1 & \beta \dfrac{\partial G_A}{\partial N} \\ 0 & 0 & 0 & 0 & \dfrac{\partial G_N}{\partial A_r} & -1 \end{pmatrix} \tag{25}$$

where

$$J_{33} = -\zeta_2 - \eta_2 g_{22} \frac{\partial F_{22}}{\partial H_2} P_2 - \eta_3 g_{23} \frac{\partial F_{23}}{\partial H_2} P_3,$$

and the dependencies of g_{ij} and F_{ij} are dropped for lack of space. The block structure of the matrix allows to say that its eigenvalues are those of the three 2×2 diagonal blocks. The first two have both negative real eigenvalues. So, the stability properties of the equilibria only depend on the last block and in particular on the sign of its determinant, being the trace of this sub-matrix constantly negative. Hence, the equilibrium state is stable if and only if

$$\frac{\partial G_A}{\partial N}\left(\alpha + G_N(A_r^{eq})\right) \frac{\partial G_N}{\partial A_r}(A_r^{eq}) < \frac{1}{\beta},$$

which obviously simplifies to

$$\frac{\partial G_N}{\partial A_r}(A_r^{eq}) < \frac{1}{\beta},$$

if $G_A(N) = N$. In this respect, when there are no turning points, as in the rightmost (blue) curve in Fig. 3b,c, then there is a unique equilibrium point which is stable. On the other hand, when there is an S-shaped equilibrium curve, like in the other curves in Fig. 3b,c, the middle branch (corresponding to decreasing values of N^{eq} as a function of Γ_A) refers to an unstable equilibrium, while the upper and lower increasing branches correspond to stable equilibria. This

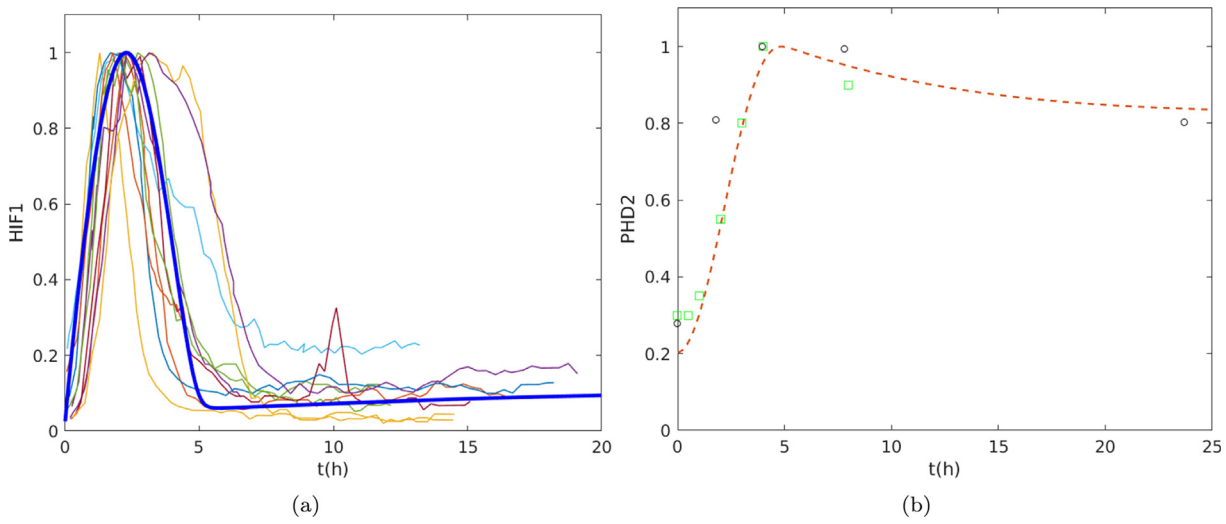

Fig. 4. HIF1 and PHD2 temporal evolution. The system is suddenly de-oxygenated into hypoxia (1% O_2) starting from a normoxic conditions (21% O_2). (a) Experimental HIF1 data on HeLa cells reported in [4] normalized with respect to their maximum values. Each curve refers to a different HeLa cell. The thick blue curve refers to the numerical result obtained using the parameters reported in Table 1. (b) Normalized PHD2 evolution compared with the temporal data reported in [4] (black circles) and with the experiments by Holmquist et al. [36] (green squares) on neuroblastoma cells.

gives rise to a condition of bistability, that potentially describes the influence of hypoxia dynamics on the switch between the onset of an acute or chronic inflammation. All the different scenarios linking hypoxia and inflammation are discussed in detail in Section 5. In the following the upper branch will be called inflammatory branch, because it corresponds to high levels of NFkB expression.

4. Time evolution

Before addressing the entire pathway reported in Eqs. (10)–(15), it is important to focus on the kinetics of HIF1 and PHD2 only, that are the most studied in the literature. Then, we will include HIF2 and PHD3 to conclude with the dynamics of the full problem discussing the possible scenarios linking hypoxia and inflammation.

4.1. HIF1-PHD2 kinetics

Focusing on Eqs. (10) and (11), we will now use experimental data (i) to check the fitting between experimental data and model output on the kinetics of HIF1 and PHD2 and (ii) to better estimate the production rates of the two chemicals, which in the literature have been so far evaluated through preliminary simulations only (see [4,12,18]). Then, being aware of the variability of response from tissue to tissue and even from cell to cell within the same cell type, we will analyze the dependence of the response on the parameters.

4.1.1. Comparison with experiments

As discussed in the Appendix and reported in Table 1, all parameters related to the HIF1-PHD2 kinetics can be identified on the basis of experiments, with the notably exception of γ_1 and γ_{21} for which we only have computational estimates [4,12,18]. To obtain a better parameter identification, we start from the experimental data reported by Bagnall et al. [4]. In their work HeLa cells were transiently cotransfected with HIF1α-EGFP and imaged by time-lapse confocal microscopy every 5 min after a drop in oxygen saturation from 20.9% to 1%.

In Fig. 4a the evolution of the HIF1 level in different cells is reported normalizing the fluorescence data with respect to their maximum. In fact, Bagnall et al. [4] advice that the quantitative fluorescence output among separate experiments or among cells in the same experiment are not comparable for reasons mainly related to fluorescence calibration in the experimental protocol and to the method of transient transfection which normally leads to different basal HIF content estimation.

From these experimental data it can be observed that the response differs even among cells of the same lineage. The output of our model with the reference values of parameters reported in Table 1 is represented by the thick blue curve in Fig. 4a that falls in the middle of the experimental curves. Fig. 4b shows a comparison of the normalized level of PHD2 with respect to the data reported in [4] for a single cell using the same parameters used in Fig. 4a. It can then be observed that the temporal evolution of both HIF1 and PHD2 obtained by the model compares well with the experimental values in terms of (i) time to reach the maximum expression, (ii) duration of HIF1 over-expression, as reported in Fig. 4a, (iii) time of maximum expression of PHD2, (iv) PHD2 overshooting, and (v) ratio of asymptotic PHD2 concentration versus its maximum value, as reported in Fig. 4b. As mentioned in the Appendix, the trend for large times (compared to the maximum concentration of HIF1, due to the normalization experimental needs) is instead used to estimate γ_1, which is the only parameter relative to HIF1-PHD2 dynamics that has not been experimentally quantified. In Fig. 4b we also report the data from experiments on neuroblastoma cells performed by Holmquist et al. [36] that show a similar trend without any further adjustment of the parameters, despite the difference in cell type used.

4.1.2. Dependence of the evolution from the parameters

Since HIF response depends on tissue and presents even differences from cell to cell, we turn out to analyze how HIF1-PHD2 dynamics depends on the dimensionless parameters, that are shown in Table 1.

In order to show the effect of the three parameters present in the subsystem (10)–(11), in Fig. 5 we report the result of some sample simulations that differ by a single parameter value. All simulations start from initial conditions for which the system is at equilibrium in a normoxic situation with $\hat{O}_2 = 210\,\mu M$ corresponding to 21% O_2 (i.e., $O_2 = 2.1$) and HIF1 and PHD2 levels given by Eq. (17). Then, for $t > 0$ the system is put into hypoxia suddenly decreasing the values of oxygen down to $\hat{O}_2 = 10\,\mu M$, corresponding to 1% O_2 (i.e., $O_2 = 0.1$). As a consequence, HIF1 starts its over-expression and PHD2 follows on a slower time scale to control HIF1 expression. So, after an overshoot, HIF1 and PHD2 levels tend to the new equilibrium corresponding to the hypoxic state, again given by Eq. (17), for the hypoxic value of O_2.

In the first row of Fig. 5, we focus on what happens when η is changed. This parameter is mainly affected by the PHD2 regulation mechanism of HIF1. Increasing η from the reference value leads to less pronounced peaks with the instant of maximum expression of

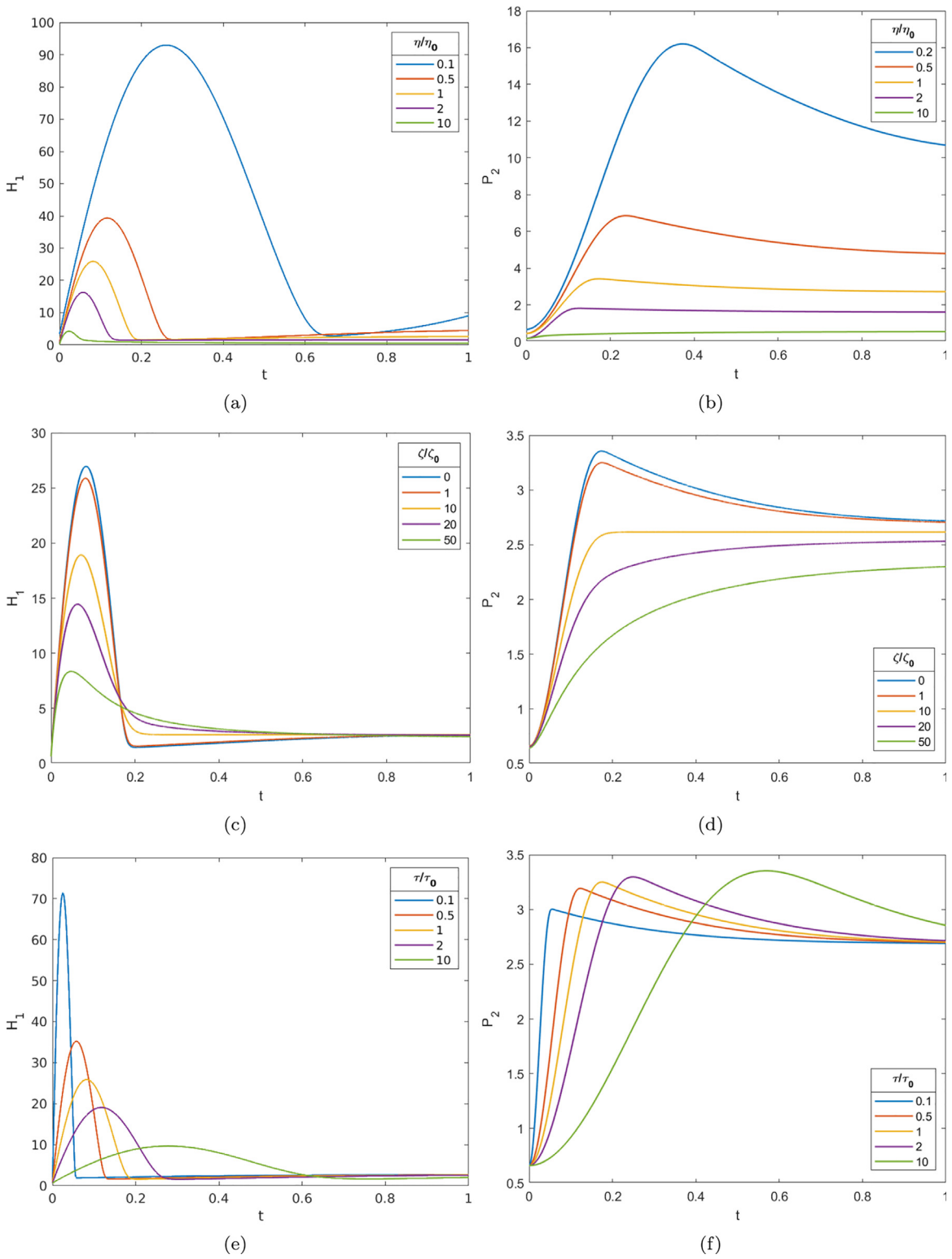

Fig. 5. Temporal evolution of HIF1 (left) and of PHD2 (right) starting from the reference values $\eta_0 = 5.6$, $\zeta_0 = 1.4 \cdot 10^{-3}$, and $\tau_0 = 1.4 \cdot 10^{-3}$. Increments in η (first row), ζ (second row), and τ (third row) all lead to less pronounced HIF1 peaks.

HIF1 achieved earlier. Conversely, decreasing η considerably increases the maxima and makes the slight undershoot after the peak more pronounced. The presence of a minimum and then a slowly increasing tendency to reach the equilibrium value also seems to be present in some experimental behaviors [4].

In the second row, we focus on the effect of ζ, that, as already discussed when dealing with the equilibria, can be neglected. First of all, we notice that the characteristic peak in HIF1 response is also present in the limit case $\zeta = 0$, that is, if the oxygen-independent degradation of HIF1 is not taken into account at all, as for instance done in [18]. Then, only increments of ζ of (at least) one order of magnitude give rise to a valuable difference in the evolution with an anticipation of the peak and a lowering of the maximum as occurs when η is increased.

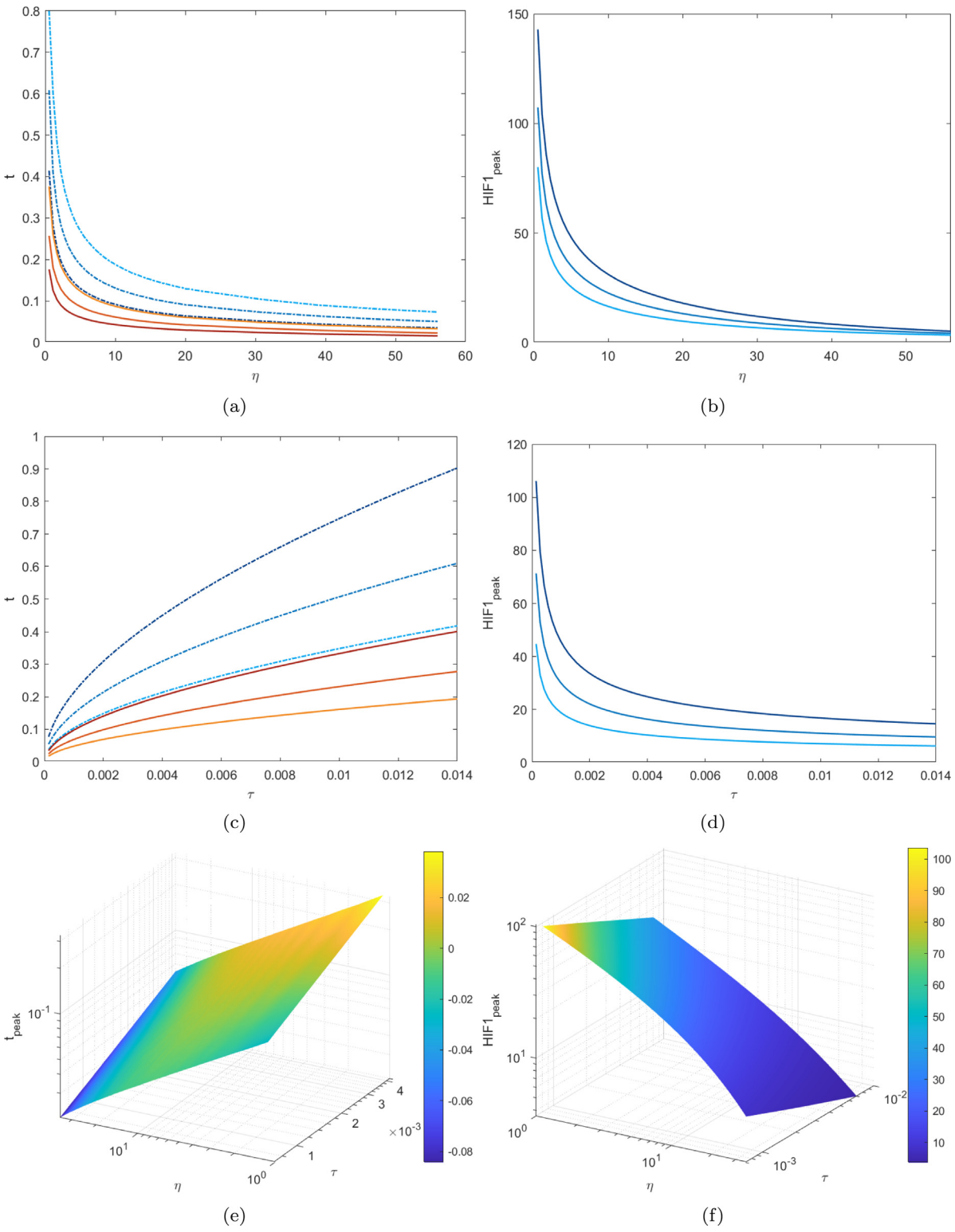

Fig. 6. On the left, dimensionless time t_{peak} to reach the maximum HIF1 activation (full red curves) and the temporal duration t_{over} of HIF overexpression (dashed blue curves). On the right: maximum dimensionless value of HIF1 activation. Top row, as a function of η when $\tau/\tau_0 = 0.5, 1, 2$ with $\tau_0 = 1.4 \cdot 10^{-3}$, from bottom to top in (a) and from top to bottom in (b). Middle row, as a function of τ when $\eta/\eta_0 = 0.5, 1, 2$ with $\eta_0 = 5.6$, from top to bottom. In the bottom row data are plotted in logarithmic scale. In (e) t_{peak} data form an almost planar surface. In this respect, colors refer to the relative error with respect to the fitting rule (26). In all cases the value of ζ is set to $\zeta_0 = 1.4 \cdot 10^{-3}$.

Finally, looking at the third row, it can be observed that increments in τ (that can, for instance, be obtained by increasing the degradation rate of PHD2 or by decreasing the production rate of HIF1) lead to slower responses, with lower peaks. So, overall increasing η and τ will both lead to a decreased activation, but in the former case the peak is anticipated and in the latter is delayed.

In Fig. 6 we focus instead on the dependence on the parameters of (i) the time t_{peak} needed to reach the maximum HIF1 expression, (ii) the duration t_{over} of HIF1 overexpression, identified by the instant of achievement of the maximum convexity, after which the dynamics slow down to reach the asymptotic value, and (iii) the maximum overexpression of HIF1 (H_1^{peak}). Referring to [37] for more details, it is

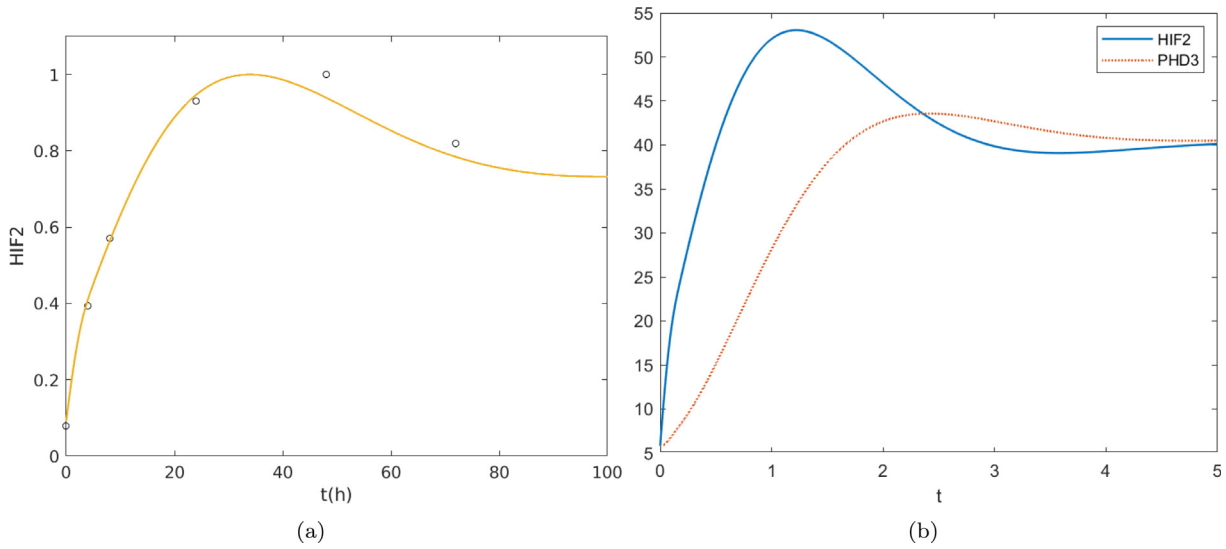

Fig. 7. HIF2 temporal evolution. The system is suddenly de-oxygenated into hypoxia (1% O_2) starting from a normoxic conditions (21% O_2). In (a) red circles represent experimental HIF2 data on breast cancer cells reported in [5] normalized with respect to the maximum value measured after 48 h. The blue curve refers to the numerical result obtained using the parameters reported in Table 1 then normalized with respect to the maximum value achieved after 33.5 h from the onset of hypoxia. (b) Dimensionless evolution of HIF2 and PHD3.

found that they all decrease upon increments in η (see Fig. 6a,b). On the contrary, t_{peak} and t_{over} increase as the value of τ increases (see Fig. 6c). The data of t_{peak} and t_{over} plotted in a log–log scale in a one order of magnitude region around η_0 and τ_0, put in evidence the existence of a power law with similar exponents both as a function of η when τ is fixed and vice versa. Actually, the results are well approximated by

$$t_{peak} \approx 5.18\sqrt{\frac{\tau}{\eta}} \qquad \text{and} \qquad t_{over} \approx 11.2\sqrt{\frac{\tau}{\eta}}, \tag{26}$$

(see Fig. 6c) with larger errors for smaller values of η's. In particular, for the reference values τ_0 and η_0, $t_{peak} \approx 0.0819$ and $t_{over} \approx 0.178$, which is a bit more than twice t_{peak}. From the definition of the dimensionless parameters, it can be noticed that the dimensional parameters γ_1 and K_{12} do not affect the characteristic times of HIF1 activation in (26). In fact, despite they are included in the definition of both τ and η, we have that

$$\sqrt{\frac{\tau}{\eta}} = \frac{\delta_{P_2}}{\sqrt{\gamma_{21}\delta_{12}^{ox}}}.$$

In the right column of Fig. 6 we focus on the maximum overexpression of HIF1 (H_1^{peak}) observing that it decreases with both η and τ. Referring again to [37] for more details, it is found that at variance from the dependence of the times in (26), the dependence from η does not seem to follow a power law as evident from Fig. 6f. However, keeping η constant, H_1^{peak} decreases like $\tau^{-0.46}$, so that we can write

$$H_1^{peak} \approx \frac{C(\eta)}{\tau^{0.46}}.$$

4.2. HIF2 and PHD3 kinetics

Though the kinetics and evolution of HIF2 is not so deeply studied, it is known that HIF2 generally takes much longer to activate when hypoxia starts, with the peak delayed by a period that ranges from several hours up to two days (see, for instance, [5,27,36]).

In Fig. 7a we report the experimental data on the evolution of HIF2 measured by Wenger et al. [5] after 6, 12, 24, 48, and 72 h from the onset of hypoxia, normalized with respect to the maximum value they measured after 48 h from the onset of hypoxia. In the same figure we superimpose the evolution resulting from the integration of (10)–(15) using the parameters reported in Table 1 and discussed in the Appendix. In particular,

$$\eta_{20} = 1.3067, \quad \zeta_{20} = 0.005, \quad \tau_{20} = 0.005 \quad \eta_{30} = 0.1.$$

In this case the value of H_2 is normalized with respect to the maximum value it achieves after 33.5 h from the onset of hypoxia yielding a qualitatively good comparison.

Fig. 7b reports the temporal behavior of both HIF2 and PHD3. Recalling that the reference evolution of HIF1 is given by the yellow curves in Fig. 5, and in particular that $t_{peak} \approx 0.0819$, it is evident how the response of activation of HIF1 and HIF2 to a sudden drop of oxygen availability follows different timing. In fact, in dimensional terms HIF1 reaches its maximum level after 2.16 h and HIF2 after 33.5 h. We also observe that the period of overexpression follows a similar slower characteristic time.

Fig. 8 focuses on the dependence of HIF2-PHD3 dynamics on the parameters. In particular, it is shown that the activation time decreases with η_2 (a), η_3 (b) and ζ_2 (c) while it increases with τ_2 (d).

Finally, Fig. 9 investigates the scenario in which normoxia is restored after a dimensionless time $t = 3$. In this case, it can be put in evidence that both H_1 and H_2 present an undershoot while the characteristic times needed to approach the asymptotic value remain similar. The behavior presented is qualitatively similar to the one reported in the experiments by Leedale et al. [12].

5. Hypoxia-inflammation dynamics and scenarios

In discussing the relation between hypoxia and inflammation mediated by HIF response, we recall that the bifurcation diagram related to alarmin receptors and NFkB might be characterized by a saddle–node bifurcation and by two turning points when $\Gamma_A = \bar{\Gamma}_1, \bar{\Gamma}_2$. This can lead to sudden activation and deactivation of the inflammatory response if the value of $\Gamma_A(t)$, that is strongly related to the expression of both HIFs and therefore to the oxygen level, varies in suitable ranges. Specifically, if, for instance, the system is in a non inflammatory state, corresponding to the lower branch, and the evolution of HIFs is such that $\Gamma_A(t)$ overcomes the value $\bar{\Gamma}_2$, then the system jumps to the upper branch triggering an overexpression of NFkB and therefore an

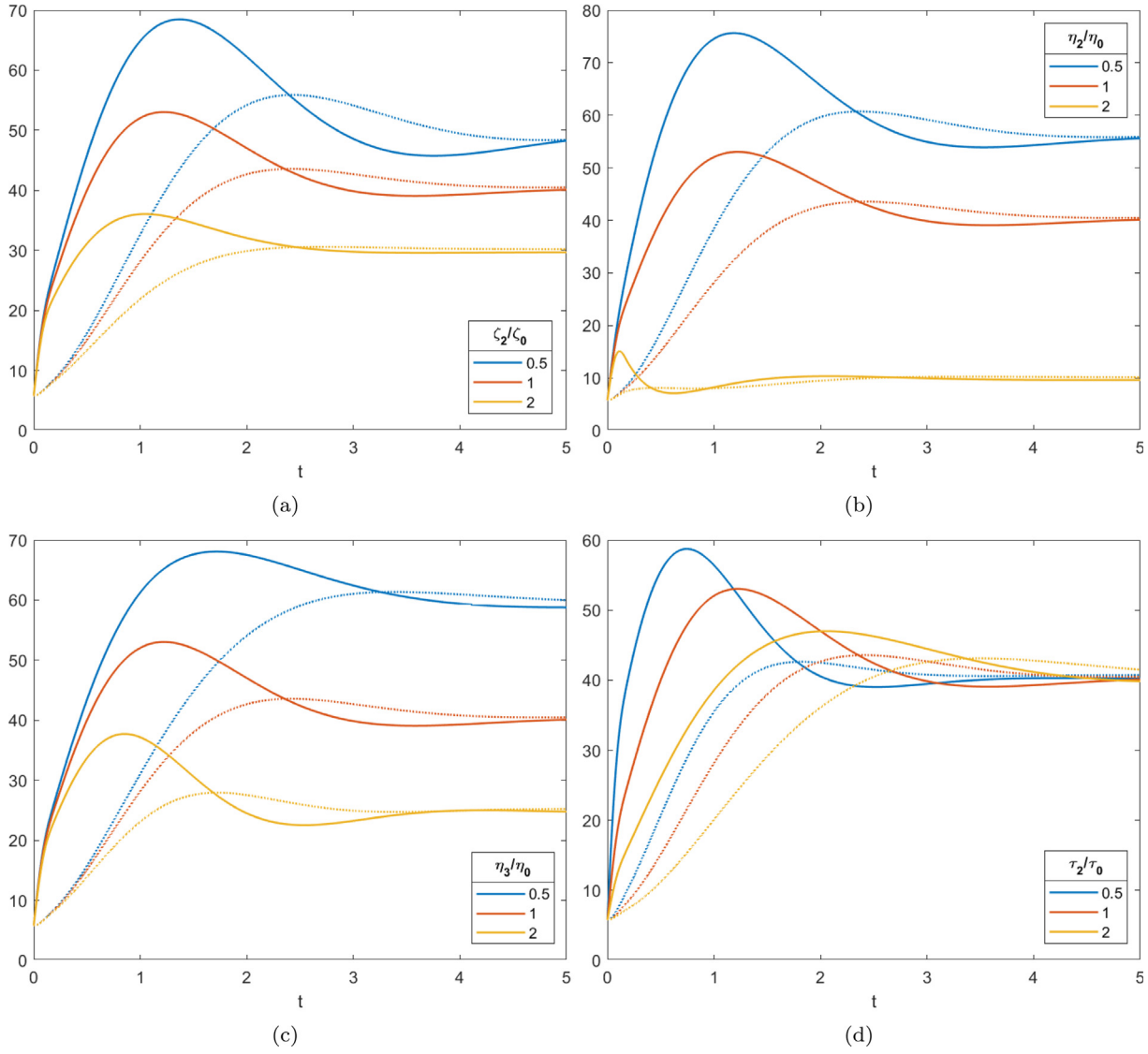

Fig. 8. HIF2 and PHD3 response to hypoxia (O_2 = 1%) starting from normoxic conditions with O_2 = 21% when (a) $\zeta_2/\zeta_{20} = 0.5, 1, 2$ (bottom to top) with $\zeta_{20} = 0.005$; (b) $\eta_2/\eta_{20} = 0.5, 1, 2$ (bottom to top) with $\eta_{20} = 1.3067$; (c) $\eta_3/\eta_{30} = 0.5, 1, 2$ (bottom to top) with $\eta_{30} = 0.1$; (d) $\tau_2/\tau_{20} = 0.5, 1, 2$ (bottom to top) with $\tau_{20} = 0.005$. The other parameters are given in Table 1.

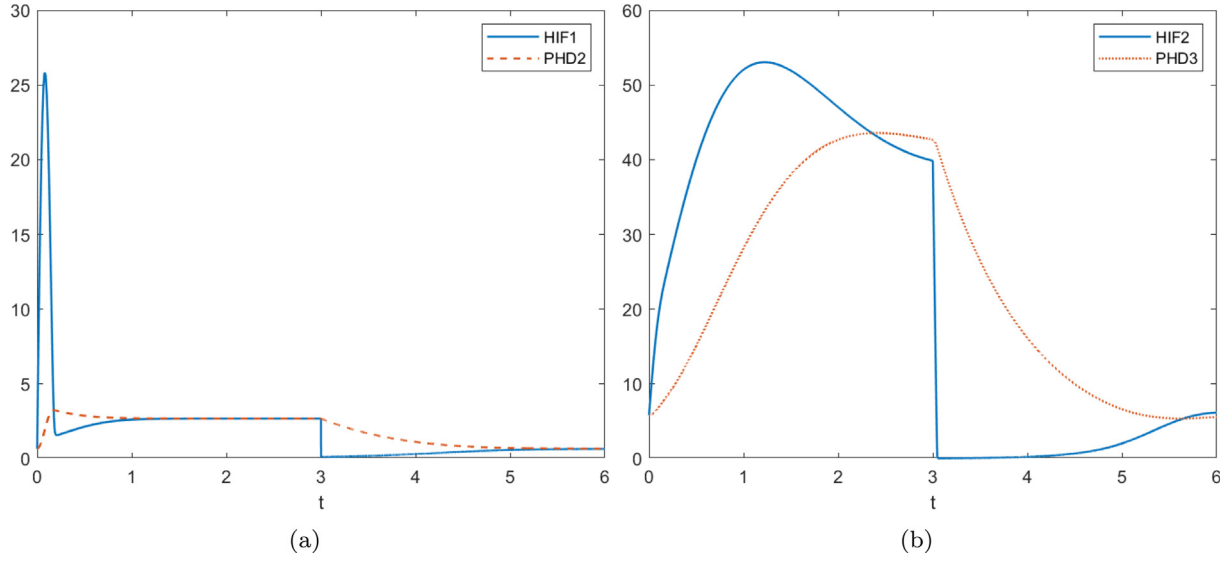

Fig. 9. HIF1, PHD2, HIF2, and PHD3 response to hypoxia (O_2 = 1%) starting from a normoxic condition with O_2 = 21% that is re-established at $t = 3$ (corresponding to 83.33 h).

Case	$\Gamma_M^1 < \bar{\Gamma}_2$	$\Gamma_m < \bar{\Gamma}_1$	$\Gamma_M^2 < \bar{\Gamma}_2$	$\Gamma_A^\infty < \bar{\Gamma}_1$	Response
N	yes	yes/no	yes	yes/no	no inflammation
A1	no	yes	yes	yes/no	early-acute
A2	yes	yes/no	no	yes	late-acute
A1*	no	no	yes	yes	acute
A12	no	yes/no	no	yes	acute
C1	no	no	yes	no	chronic
C2	yes	yes/no	no	no	chronic
C12	no	yes/no	no	no	chronic

(a)

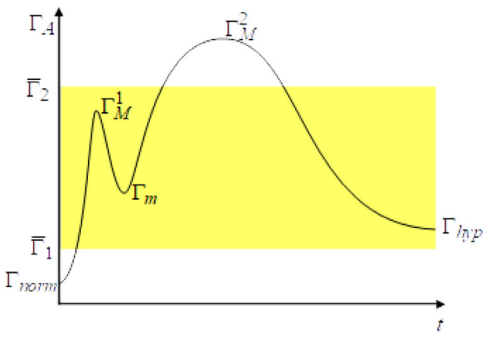

(b)

Fig. 10. (a) Inflammatory scenarios according to the relative position of maxima, minimum, and equilibrium values of $\Gamma_A(t)$ with respect to the values $\bar{\Gamma}_1$ and $\bar{\Gamma}_2$ of the turning points. "Yes" and "no" refer respectively to whether the inequality in the first row is satisfied or not, while "yes/no" means indifference. "A" and "C" in Cases stand respectively for acute and chronic. The following 1 and or 2 refer to whether HIF1 and/or HIF2 are responsible of the inflammatory state. Early-acute responses only last during HIF1 activation, late-acute responses only during HIF2 activation, acute responses span over both activation periods and chronic responses go on if hypoxia persists. (b) Example of evolution of $\Gamma_A(t)$ in Case C2.

inflammatory response. Vice versa, if the system is in an inflammatory state, corresponding to the upper branch and the evolution of HIFs is such that $\Gamma_A(t)$ drops below the value $\bar{\Gamma}_1$, then the system jumps to the lower branch corresponding to an underexpression of NFkB and therefore to a resolution of the inflammation.

Now, the combination of HIF1 and HIF2 evolution can be rather complicated, so that, as sketched in Fig. 10b, the evolution of $\Gamma_A(t)$, that in our simulations is taken to be a linear combination of $H_1(t)$ and $H_2(t)$, i.e.,

$$\Gamma_A(t) = p[H_1(t) + rH_2(t)] \qquad \text{with} \qquad p = \frac{\gamma_{A1} K_{12}}{\delta_A K_A} \qquad \text{and} \qquad r = \frac{K_{23}}{K_{12}}\rho, \tag{27}$$

might present two peaks: the former builds up in a couple of hours and corresponds to HIF1 activation, the latter builds up after nearly a day and corresponds to HIF2 activation. The relative importance of the two peaks crucially depends on the ratio r that mediates the relative sensitivity of alarmin receptor expression to HIF1 and HIF2.

Several scenarios are then possible according to whether (i) the peak of HIF1 and/or of HIF2 are such that for some time intervals $\Gamma_A(t) > \bar{\Gamma}_2$, (ii) the local minimum in between the two peaks (if present) drops below $\bar{\Gamma}_1$, and (iii) the equilibrium value eventually reached in hypoxic and normoxic conditions is above or below $\bar{\Gamma}_1$.

To discuss the possible scenarios, assuming that the evolution of $\Gamma_A(t)$ has two peaks, we hereafter denote by Γ_{norm} the value of Γ_A in normoxic conditions, by Γ_{hyp} its value in hypoxic conditions, by Γ_M^1 and Γ_M^2 the two maximum values, and by Γ_m the local minimum value (see Fig. 10b). Referring to the Table in Fig. 10a, we will denote the temporary inflammatory responses as *early-acute* when it lasts for few hours (essentially triggered by HIF1 activation only, i.e., Case A1), *late-acute* when it lasts for several hours starting after few hours (essentially triggered by HIF2 activation only, i.e., Case A2), and simply *acute* when it lasts several hours but starts sooner (due either to both activations, i.e., Case A12, or to an HIF1 activation that does not fade enough, i.e., Case A1*). Finally, an inflammatory state that asymptotically persists is called *chronic*. In the Table in Fig. 10a Case C1 refers to the situation in which it is triggered by HIF1, C2 when it is triggered by HIF2, and C12 when it is due to both. It is important to notice that if the value of Γ_A in normoxic conditions is such that $\Gamma_{norm} > \bar{\Gamma}_1$, then, as discussed in the following, the chronic inflammation might pathologically persist also in the case of restored normoxia.

In order to focus in more detail on the case in which bistability occurs, in the simulation we set $\beta = 1.9$ and $\alpha = 0$, assuming a negligible basal production of NFkB, as done in [22]. Furthermore, the normoxic parameters are such that the system initial condition falls in the lower branch of the bifurcation diagram represented in Fig. 3.

Let us start the description of the possible scenarios by focusing first on the case of a fast response, that can be obtained with suitably small τ_A and τ_N, so that the dynamics of A_r and N readily follow the bifurcation curve.

In the case in which alarmin receptors are only triggered by one HIF isoform (e.g., HIF1 corresponding to taking $\gamma_{A2} = 0$), $\Gamma_A(t)$ has only one maximum and the dynamics is simpler. Of course, the inflammatory response is triggered if $\Gamma_M^1 > \bar{\Gamma}_2$ and lasts for a period similar to the overexpression of HIF1 if Γ_{hyp} drops below $\bar{\Gamma}_1$, as shown in Fig. 11a. So, even though hypoxia persists, the inflammatory response is temporary. This graphically corresponds to the situation in which, starting from the lower branch, the system jumps to the upper inflammatory branch because Γ_A has overcome the turning point. However, when the overshoot of HIF1 is over, the systems jumps back to the lower non-inflammatory branch. On the other hand, if $\Gamma_{hyp} > \bar{\Gamma}_1$, then the system chronically remains in the inflammatory state, corresponding to the upper branch, also when HIF overexpression is over, leading to a persistent inflammatory response as shown in Fig. 11b (Case C1).

In the most general case of an influence of both HIF1 and HIF2 on alarmin receptor expression, if, for instance, the two maxima of $\Gamma_A(t)$ do not overcome the threshold $\bar{\Gamma}_2$, i.e., in Case N of Table in Fig. 10a, then the system configuration is constantly in a state corresponding to a point on the lower branch and inflammation is never triggered.

Instead, in the case in which the HIF2-related peak leads to $\Gamma_A(t) > \bar{\Gamma}_2$ for some time, then, when HIF2 overexpression starts, the system will jump to the upper inflammatory branch, leading to a late-acute inflammation that lasts till the end of HIF2 overexpression, if the asymptotic value of $\Gamma_A(t)$ is lower than $\bar{\Gamma}_1$, i.e., in Case A2, because the level of $\Gamma_A(t)$ drops below criticality. However, as before the inflammatory state can become chronic if $\Gamma_{hyp} > \bar{\Gamma}_1$, i.e., in Case C2 of the Table in Fig. 10a. This scenario is the one reported in Fig. 12a that shows that HIF1 overexpression does not lead to an inflammatory response, as it is evident from the fact that NFkB is underexpressed in the early stages of hypoxia, but the activation of HIF2 will generate a late inflammatory response that is also chronic. The figure also highlights how the jump in NFkB expression corresponds to the instant in which $\Gamma_A > \bar{\Gamma}_2$ (see the yellow curve). This inflammatory state will stop only after normoxia

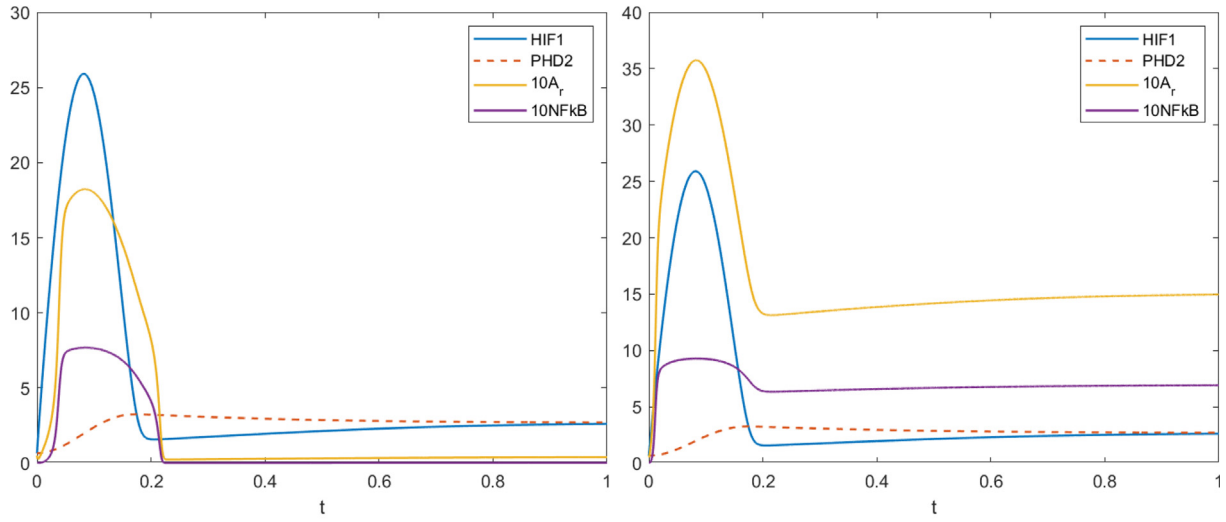

Fig. 11. Temporal evolution of HIF1, PHD2, NFkB and alarmin receptor expression when the inflammatory response is only influenced by HIF1 ($r = 0$). (a) Early-acute inflammation ($p = 0.014$). (b) Chronic inflammation ($p = 0.07$).

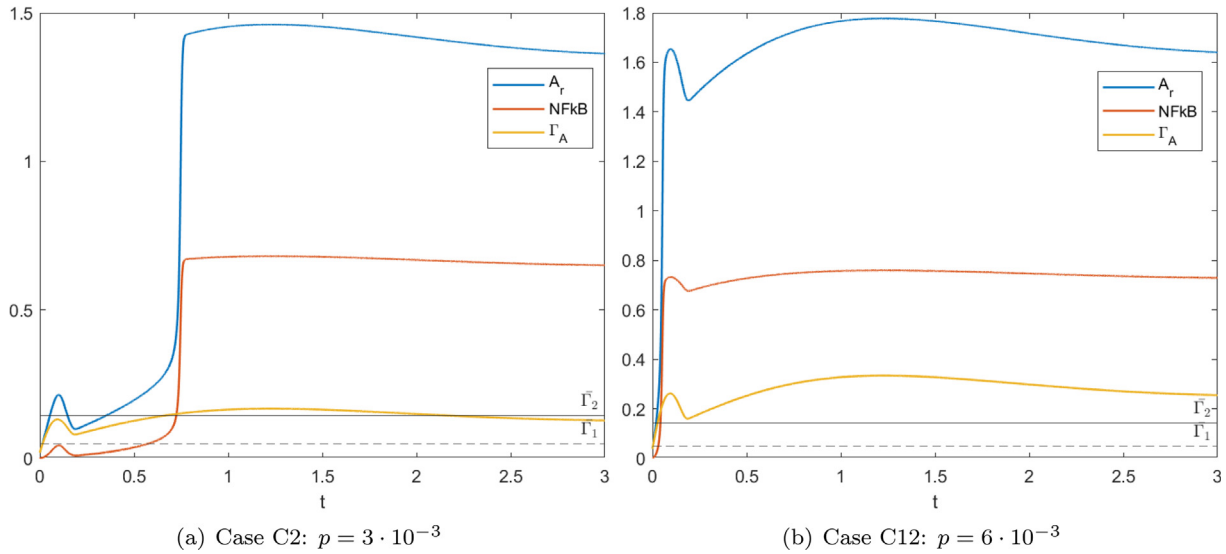

Fig. 12. HIFs, NFkB and alarmin signaling temporal evolution. (a) Late-acute inflammation caused by HIF2 activation, corresponding to Case C2 ($p = 3 \cdot 10^{-3}, r = 1$). (b) Acute inflammation caused by both HIF1 and HIF2 activation, corresponding to Case C12 ($p = 6 \cdot 10^{-3}, r = 1$). The evolution of HIF1, HIF2, PHD2 and PHD3 is given in Fig. 8a,b. The gray dashed and full lines correspond respectively to $\bar{\Gamma}_1 = 0.0487$ and $\bar{\Gamma}_2 = 0.1437$.

is restored if $\Gamma_{norm} < \bar{\Gamma}_1$. Otherwise, as already stated, in principle the system might remain in the upper inflammatory branch also in normoxic conditions. However, as will be discussed in the following, the presence of a temporary undershoot when normoxic conditions are restored (as in Figs. 9 and 13) might help stopping the inflammatory response.

If also the HIF1-related peak is higher than $\bar{\Gamma}_2$, as in Cases A1* and C12 of Table in Fig. 10a, then the inflammatory state starts earlier, i.e., just after HIF1 activation, and lasts longer (see Fig. 12b). In these cases we have what we have previously called respectively an acute and a chronic inflammation that, however, will start earlier with respect to the just discussed Case C2. Notice again that the jump of overexpression corresponds to the crossing of Γ_A over the line $\bar{\Gamma}_2$. Similar dynamics occur in Cases A12 and C12. We notice that in Fig. 12 we only changed the parameter p to go from the scenario on the left to that on the right.

To complete the possibilities, in Case A1 of the table in Fig. 10a the overcome of $\bar{\Gamma}_2$ is determined by the peak of HIF1. However, the fact that the local minimum drops below $\bar{\Gamma}_1$ implies that the system soon goes back to the lower branch and the small response to HIF2 is not able to start again the inflammation. That is why we named these dynamics *early-acute*. In this case, the evolution is similar to the one reported in Fig. 11a.

In Fig. 13, we focus on the behavior of the system when normoxia is restored at the dimensionless time $t = 2$. As in Fig. 9 this causes the presence of a strong undershoot that likely makes $\Gamma_A(t)$ drop below $\bar{\Gamma}_1$ and therefore the system may jump to the non-inflammatory branch and stay there even if $\Gamma_{norm} > \bar{\Gamma}_1$. If the undershoot is not strong enough, then inflammation persists even if normoxia is restored.

On the other hand, we explicitly observe that if $\bar{\Gamma}_1 < 0$ (corresponding to Case III of Fig. 3a with $\beta \geq 2$), then the inflammatory state is irreversible. In fact, even nullifying Γ_A, the system would remain in an inflammatory configuration corresponding to the upper branch. In this latter case the only way to resolve inflammation would be to operate in such a way that $\bar{\Gamma}_1$ is brought back to a positive value. To be specific

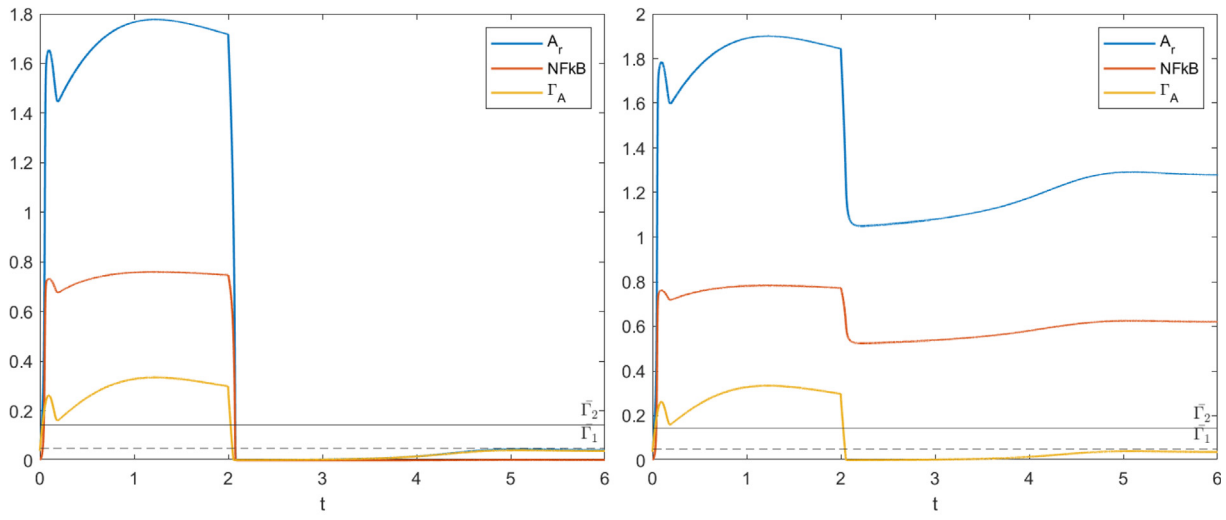

Fig. 13. Temporal evolution of HIFs, PHDs, NFkB and alarmin receptor expression in hypoxia and after reoxygenation at dimensionless time $t = 2$. (a) For $\beta = 1.9$ inflammation ends after reoxygenation. (b) For $\beta = 2$ inflammation persists even after reoxygenation. The gray dashed and full lines correspond respectively to $\bar{\Gamma}_1 = 0.0487$ and $\bar{\Gamma}_2 = 0.1437$. In both simulations $p = 6 \cdot 10^{-3}$ and $r = 1$.

and referring to Fig. 3, keeping $\alpha = 0$, then β must achieve values smaller than 2, which can be obtained, for instance, increasing the NFkB-induced expression of alarmin receptors (γ_{AN}), or the sensitivity of NFkB to their signaling (γ_{NA}), or decreasing their degradation rates δ_A and δ_N.

Referring to these cases, Fig. 13 shows how the asymptotic behavior drastically changes by simply changing β from 1.9 (left) to 2 (right). In fact, referring to Fig. 3 in the former case $\bar{\Gamma}_1 > 0$ and in the latter case $\bar{\Gamma}_1 = 0$. We remark that the evolutions of $H_1(t)$, $H_2(t)$, and $\Gamma_A(t)$ are the same in both cases, with the existence of a relevant underexpression after re-oxygenation at $t = 2$. So, in Fig. 13a inflammatory response resolves because the value of $\Gamma_A(t) < \bar{\Gamma}_1$ right after $t = 2$. On the contrary, in Fig. 13b this cannot occur because for $\beta = 2$ we are in Case III of Fig. 3a. As a result, the system remains in the upper inflammatory branch also in normoxic condition and the inflammatory response still persists.

A different dynamics may occur if the characteristic response times of HIF1 and HIF2 are comparable. In this case the two peaks sum up yielding a higher maximum. So, it might happen that, when separated, the two peaks are not able to trigger inflammation because they are both below threshold, but their pathological and synergistic merging could. At this point the possibility that inflammation can become chronic depends again on whether eventually Γ_A is larger or smaller than $\bar{\Gamma}_1$.

Another phenomenon can occur when τ_A and τ_N are sufficiently large, so that the dynamical inflammatory response is slower than HIF activation. In this case it might happen that, though $\Gamma_M^1 > \bar{\Gamma}_2$, the fact that HIF1 overexpression only lasts few hours implies that there is not enough time to overexpress alarmins and activate NFkB. On the other hand, since overexpression of HIF2 lasts much longer, if the hypoxic state lasts so long to persist during HIF2 overexpression, then there is enough time to trigger the inflammatory response. On the contrary, if it is only temporary (e.g., few hours) then there is no inflammatory response at all. In this respect, Fig. 14 shows how the activation time of NFkB increases with τ_N. Specifically, with respect to the reference curves characterized by steeper slopes and overshoots of A_r and N, an increase by one order of magnitude of τ_N leads to a slightly slower response and a loss of the overshoot. An increase by one order more leads to a response that is insensitive to HIF1 peak dynamics and that develops after a time that characterizes HIF2 response. The same behavior is observed when τ_A is changed (not shown).

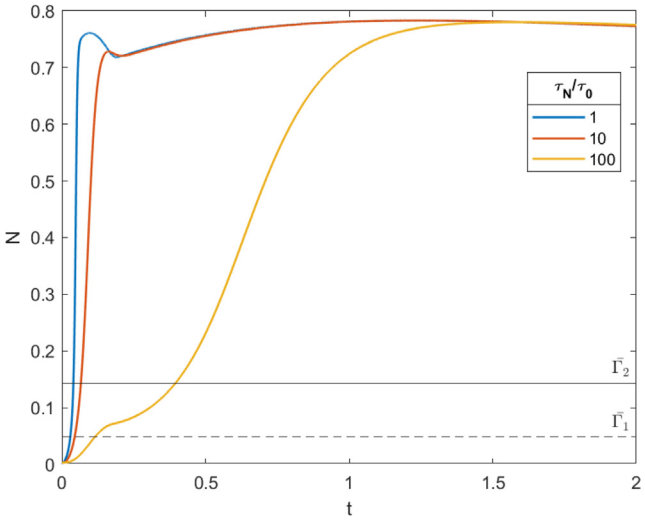

Fig. 14. NFkB temporal evolution when $\tau_N/\tau_0 = 1, 10, 100$ with $\tau_0 = 10^{-3}$, $p = 6 \cdot 10^{-3}$, $r = 1$.

6. Discussion and conclusions

HIF stabilization in cancer cells promotes the acquisition of many hallmarks of malignancy, such as chronic inflammation, and it is associated with poor survival in diverse types of human solid tumors [38,39]. Since HIFs and NFkB converge on the regulation of crucial genes involved in cancer progression, it is important to further elucidate connections between hypoxic and inflammatory responses in order to target them. Indeed, an increasing number of HIF and NFkB regulators is studied in a pharmacological perspective in cancer therapy (see for instance [40–42]). Keeping this need in mind, we first modeled the dynamics of HIF and its regulators, comparing the results with available data on the main biological features summarized in Table 2. We then modeled the interplay between hypoxia and inflammation exploring different scenarios that allow to differentiate between acute and chronic inflammation and to identify the cases in which inflammatory response is self-sustaining, underlying the role that both HIFs and their connection with alarmin receptors and NFkB may play in this link.

Table 2
Summary of features of HIF and PHD dynamics and related references reporting the experimental data used for comparison. The figures mentioned without reference refer to plots focusing on the dependence of the evolution upon parameter changes.

Figure [Ref]	Features
Fig. 2a,b Fig. 2c [35]	Dependence of non-dimensional HIF1 on O_2
Fig. 4a [4] Fig. 5a,c,e Fig. 15	HIF1 temporal evolution: 1. Time of maximum expression 2. Duration of over-expression
Fig. 4b [4,36] Fig. 5b,d,f	PHD2 temporal evolution: 1. Time of maximum expression 2. Overshooting 3. Ratio of asymptotic PHD2 concentration versus its maximum value
Fig. 7 [5] Fig. 8	HIF2 temporal evolution: 1. Time of maximum expression 2. Overshooting

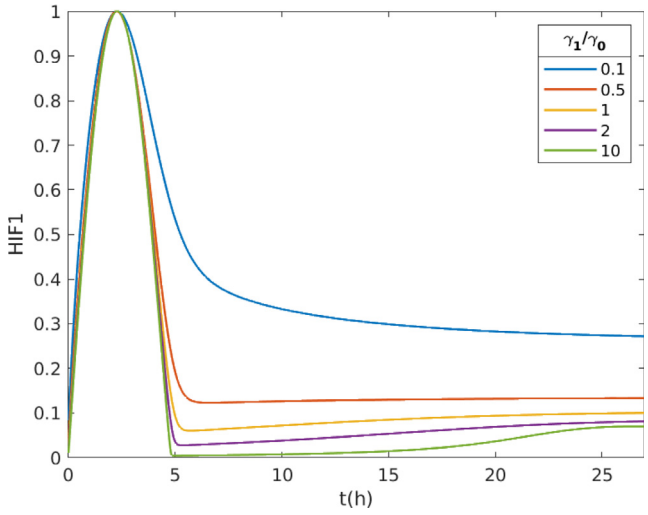

Fig. 15. HIF1 evolution normalized with respect to the maximum value as γ_1 is varied.

We have shown that the type of inflammatory response depends both on parameters affecting HIF activation in response to hypoxic conditions and on parameters describing the downstream response of alarmin receptors and NFkB to the activation above. So, one action to limit inflammation can be to control upstream HIF activation, both in terms of maximum overexpression, which may trigger inflammation by causing a jump between basins of attraction in a bistability landscape, and equilibrium level under hypoxia, which can make the inflammatory state chronic. The parameters affecting the most both aspects are η, η_2 and η_3, that is, parameters that model hydroxylation, where the first is related to HIF1 activation and the others to HIF2 activation (with η_2 less important from the biological point of view). In particular, increasing them leads to lowering both the equilibrium value under hypoxia (see Fig. 2a) and the peaks of activation (see Eq. (26), Figs. 5a, 6b,f, and 8b,c). This can be, for instance, achieved by (i) increasing the inhibitory activity of PHD2 and PHD3 upon HIF1 and HIF2 (i.e., δ_{12}^{ox} and δ_{23}^{ox}), or (ii) increasing HIF-related production of PHDs (i.e., γ_{21} and γ_{32}), or (iii) decreasing the basal production of HIFs (i.e., γ_1 and γ_2), or (iv) decreasing the basal degradation of PHDs (i.e., δ_{P_2} and δ_{P_3}). Then, this action can be for instance accomplished targeting, specifically increasing, hydroxylation (e.g., through benzopyranyl triazole) or impacting directly on hydroxylation increasing PHD activity (e.g., through ascorbate).

Another action to prevent chronic inflammation would be to keep NFkB response to HIF activation low, which is mainly related to the parameters p and r in Eq. (27), that is to the expression of alarmin receptors in response to HIF overexpression. In this respect, the role of HIF2 seems to be more important as is active for a longer period. So, if the characteristic times (related to τ_A and τ_N) are not fast enough, then the quick reaction of HIF1 can pass by before the onset of inflammation (see Fig. 14). This does not occur for HIF2 whose overexpression lasts longer. So, it would be more relevant to target the parameters related to HIF2, e.g. the product pr, rather than those more closely related to HIF1.

We have also shown that another parameter that crucially influences the interplay between hypoxic and inflammatory response is β. It describes the transcriptional activity of NFkB on genes that encode for alarmin receptors. In fact, when close to criticality, even a tiny increase of β (e.g., from 1.9 to 2) favors the onset of a chronic inflammatory state that persists even if normoxic conditions are restored. In that scenario, even a drastic decrease of HIF would not resolve inflammation and only decreasing β would allow to stop inflammation. Such a change could be addressed by pharmacologically targeting NFkB activation impacting either directly or indirectly on its transcriptional activity.

Declaration of competing interest

The authors declare that they have no known competing financial interests or personal relationships that could have appeared to influence the work reported in this paper.

Acknowledgments

This work was partially supported by Gruppo Nazionale di Fisica Matematica of INdAM, Italy, the Italian Ministry of Education, Universities and Research through the MIUR, Italy grant “Dipartimenti di Eccellenza 2018–2022” (Project no. E11G18000350001) and the Scientific Research Programme of Relevant National Interest (Project n. 2017KL4EF3).

Appendix. Model parameters

The focus of this paper is to model the change in cell behavior passing from a normoxic condition to a hypoxic or even anoxic one. However, we need to mention that the levels of oxygen saturation defining such situations are not precisely defined and differ in *in vitro* experiments w.r.t. in vivo conditions. For instance, a saturation level of about 21% of oxygen in *in vitro* experiments, which corresponds to about 210 μM [32], is generally denoted as a normoxic condition and a level of 1%, which corresponds to about 10 μM [32], as a hypoxic condition [4,30,34,36,43]. Finally, in [44] a value below 0.1% is defined as an anoxic condition. On the other hand, in both normal and pathological peripheral tissues, oxygen saturation never reaches such high values even in normoxia (e.g., arterial blood O_2 is at 13.2%). So, for instance, in [45] it is observed that normoxic values for different tissues range between 3% and 7.4%. On the other hand, it is observed that the median oxygenation of tumors falls approximately between 0.3% and 4.2%, with most tumors exhibiting median oxygen level below 2%.

Oxygen concentration enter the model through the Michaelis–Menten functions g_{ij} that are characterized by the affinity constants K_{ij}^{ox}. In early experiments, Hirsila et al. [46] found that all K_{ij}^{ox} have a similar magnitude and evaluated them to be in the range $230-250\,\mu M$. Coherently, in the models proposed by [13] and then [18] a value of 250 μM is used for K_{12}^{ox}. However, Hirsila et al. [46] used 2-oxoglutarate consumption assays and relatively short peptide substrates for HIFs, which both can lead to an overestimation of the kinetic measurements. In fact, more recent experiments using C-14 and longer peptides lowered the above value to $K_{12}^{ox} \in [70, 100]\,\mu M$ [30,32,47]. Assuming that, as just mentioned, the values of K_{23}^{ox} and K_{12}^{ox} remain similar, as stated in [46], we set as reference value $K_{23}^{ox} = 100\,\mu M$.

Instead, also in agreement with [30], we set a slightly lower value for $K_{22}^{ox} = 70\,\mu M$.

For the degradation rate δ_{12}^{ox}, we set the reference value to be $\delta_{12}^{ox} = 1 \cdot 10^{-2}\ s^{-1}$, which is an intermediate value between studies in which hydroxylation is quantified by C-14 [30] and by mass spectrometry [31]. In fact, these cited articles respectively allow to quantify hydroxylation either indirectly, e.g., from CO_2 release, or directly. In these studies the reported activation rate ranges from 0.22 to 1.16 min^{-1}, that in terms of seconds leads to $\delta_{12}^{ox} \in [3.7 \cdot 10^{-3}, 1.9 \cdot 10^{-2}]\,s^{-1}$.

Furthermore, in agreement with [30], we set $\delta_{22}^{ox} = 7 \cdot 10^{-3}\ s^{-1}$; in the absence of experimental data we set $\delta_{23}^{ox} = 10^{-4}\ s^{-1}$ in order to fit the experimental curve (see Fig. 7).

Regarding K_{12}, we recall that all HIFs have two proline residues that can be targeted by PHDs. Luckily, it was recently shown that the presence of two hydroxylated prolines, as compared to a single hydroxylated one, does not significantly affect HIF degradation [48]. This allows to model HIF1 degradation mediated by PHD2 taking just one hydroxylation into account. Considering that the measured value of K_{12} ranges then from 1 to 24 μM, mainly depending on the peptide substrate used, as just mentioned above, we use the intermediate quantity $14\,\mu M$ as the reference value for K_{12}. Similarly, on the basis of the results reported in [30,32], we respectively set $K_{22} \approx 15\,\mu M$ and $K_{23} = 150\,\mu M$.

In [12,13] the basal PHD2 degradation rate δ_{P_2} is experimentally reported to be approximately in the range $1–1.5 \cdot 10^{-5}\ s^{-1}$ and here the same value is also used for δ_{P_3} assuming a similar degradation process for the two isoforms.

On the other hand, basal HIFs degradation, described by the terms proportional to δ_i, becomes relevant only in extreme hypoxic conditions, because the hydroxylation-proteosome degradation pathway, described by the terms proportional to δ_{ij}^{ox}, becomes essentially inactive due to the lack of O_2 [44]. Coherently, in our model we assume a value of $\delta_1 = \delta_2 = 10^{-5}\ s^{-1}$ significantly lower than the one for the oxygen dependent degradation. We observe that, on the same page, Bocharov et al. [18] take an unrealistic value close to $10^{-5}\,days^{-1}$ and, actually, for its smallness, this term is even neglected in other models (as, for instance, in [4]).

The parameters related to the production terms are in general more difficult to be evaluated directly from experiments, because the results are typically given in terms of scaled (or relative) quantities that are necessarily introduced for experimental calibration purposes.

Having HIF evolutions that change from cell to cell, Leedale et al. [12] used the strategy of fitting, for any cell, the parameters of their model. In this way, for each of them they obtained a different set of parameter values that are then averaged. In particular, their model includes a rate of production of PHD2, i.e., our γ_{21}, for which they found fitting values ranging in the interval $0.5 – 4 \cdot 10^{-5}\ s^{-1}$, then averaged to $1.5 \cdot 10^{-5}\ s^{-1}$ also in [4].

Having set the remaining parameters according to other experimental studies, in Section 4.1.1 we opted for a different strategy, namely, merging all the curves and looking for production parameters fitting their behavior. This procedure led to the identification of $\gamma_{21} = 4 \cdot 10^{-5}\ s^{-1}$ as a good candidate, which is still in the range found in [12]. Then, for γ_{31} we assume the same value as γ_{21}, since they represent the same biological function, that is the transcriptional influence of HIF1 on its target genes and $\gamma_{32} = \frac{\gamma_{21}}{2} = 2 \cdot 10^{-5}\ s^{-1}$ also on the basis of the experimental results on parental MCF7 breast cancer cells obtained by Wenger et al. [5].

As discussed in Section 4.1.1, the value of the basal production of HIFs is not experimentally available, because of the necessary rescaling procedure of the measured quantities. In fact, as pointed out in the discussion after Eq. (26) the fitting of the dimensionless times characteristic of HIF activation gives a relation that is independent from γ_1. This is also demonstrated by the graph in Fig. 15, which shows that variations of γ_1 (i) do not lead to variations in the time needed to reach maximal activation and (ii) affect only slightly the duration of HIF activation. On the contrary, γ_1 significantly influences the intensity of undershooting and the ratio between the asymptotic equilibrium and the peak activation value which, however, as shown in Fig. 4, is characterized by a large variability in the empirical measures. A reasonable average of such experimental data has been obtained setting $\gamma_1 = 0.1$. Similarly, a close value of $\gamma_2 = 0.3$ has allowed to get a good fitting between numerical and empirical outcomes, see Fig. 7a, although available laboratory-based measurements relative to HIF2 are still poor with respect to those relative to HIF1.

As shown in Sections 3.1, 4.1.1, and 4.2, the proposed parameter estimate has lead to HIF and PHD temporal evolutions close to their empirical counterparts [4,35,36].

The reference dimensionless parameters regarding HIF-PHD kinetics are listed in Table 1.

Unfortunately, there are no quantitative measurements of the parameters present in Eqs. (6) and (8). For this reason, in Section 5 we discussed the possible scenarios as a function of the dimensionless groups of parameters.

References

[1] M. Pressley, J.A. Gallaher, J.S. Brown, M.R. Tomaszewski, P. Borad, M. Damaghi, R.J. Gillies, C.J. Whelan, Cycling hypoxia selects for constitutive HIF stabilization, Sci. Rep. 11 (1) (2021) 1–14.

[2] G.L. Semenza, Hydroxylation of HIF-1: oxygen sensing at the molecular level, Physiology 19 (4) (2004) 176–182.

[3] E.R. Watts, S.R. Walmsley, Inflammation and hypoxia: HIF and PHD isoform selectivity, Trends Molec. Med. 25 (1) (2019) 33–46.

[4] J. Bagnall, J. Leedale, S.E. Taylor, D.G. Spiller, M.R.H. White, K.J. Sharkey, R.N. Bearon, V. Sée, Tight control of hypoxia-inducible factor-α transient dynamics is essential for cell survival in hypoxia, J. Biol. Chem. 289 (9) (2014) 5549–5564.

[5] D.P. Stiehl, M.R. Bordoli, I. Abreu-Rodriguez, K. Wollenick, P. Schraml, K. Gradin, L. Poellinger, G. Kristiansen, R.H. Wenger, Non-canonical HIF-2α function drives autonomous breast cancer cell growth via an AREG–EGFR/ErbB4 autocrine loop, Oncogene 31 (18) (2012) 2283–2297.

[6] G.L. Semenza, Hypoxia-inducible factors in physiology and medicine, Cell 148 (3) (2012) 399–408.

[7] P. Pichiule, J.C. Chavez, A.M. Schmidt, S.J. Vannucci, Hypoxia-inducible factor-1 mediates neuronal expression of the receptor for advanced glycation end products following hypoxia/ischemia, J. Biol. Chem. 282 (50) (2007) 36330–36340.

[8] H.K. Eltzschig, P. Carmeliet, Hypoxia and inflammation, New Eng. J. Med. 364 (7) (2011) 656–665.

[9] M. Papale, M. Buccarelli, C. Mollinari, M.A. Russo, R. Pallini, L. Ricci-Vitiani, M. Tafani, Hypoxia, inflammation and necrosis as determinants of glioblastoma cancer stem cells progression, Int. J. Molec. Sci. 21 (8) (2020) 2660.

[10] M. Tafani, L. Schito, L. Pellegrini, L. Villanova, G. Marfe, T. Anwar, R. Rosa, M. Indelicato, M. Fini, B. Pucci, M.A. Russo, Hypoxia-increased RAGE and P2x7r expression regulates tumor cell invasion through phosphorylation of Erk1/2 and Akt and nuclear translocation of NF-κB, Carcinogenesis 32 (8) (2011) 1167–1175.

[11] F.R. Greten, S.I. Grivennikov, Inflammation and cancer: triggers, mechanisms, and consequences, Immunity 51 (1) (2019) 27–41.

[12] J. Leedale, A. Herrmann, J. Bagnall, A. Fercher, D. Papkovsky, V. Sée, R.N. Bearon, Modeling the dynamics of hypoxia inducible factor-1α (HIF-1α) within single cells and 3D cell culture systems, Math. Biosci. 258 (2014) 33–43.

[13] L.K. Nguyen, M.A.S. Cavadas, C.C. Scholz, S.F. Fitzpatrick, U. Bruning, E.P. Cummins, M.M. Tambuwala, M.C. Manresa, B.N. Kholodenko, C.T. Taylor, A. Cheong, A dynamic model of the hypoxia-inducible factor 1α (HIF-1α) network, J. Cell Sci. 126 (6) (2013) 1454–1463.

[14] Y. Yu, G. Wang, R. Simha, W. Peng, F. Turano, C. Zeng, Pathway switching explains the sharp response characteristic of hypoxia response network, PLOS Comput. 3 (8) (2007) e171.

[15] A.A. Qutub, A.S. Popel, Three autocrine feedback loops determine HIF1α expression in chronic hypoxia, 1773 (10) (2007) 1511–1525.

[16] P.J. Robinson, Hack C.E., Mathematical model of HIF-1α pathway, oxygen transport and hypoxia, AFRL-RH-WP-TR-2017-0080.

[17] B. Schmierer, B. Novák, C.J. Schofield, Hypoxia-dependent sequestration of an oxygen sensor by a widespread structural motif can shape the hypoxic response - A predictive kinetic model.

[18] G. Bocharov, W. Jäger, J. Knoch, M. Neuss-Radu, M. Thiel, A mathematical model of HIF-1 regulated cellular energy metabolism, Vietnam J. Math. 49 (1) (2021) 119–141.

[19] C. Kelly, K. Smallbone, M. Brady, Tumour glycolysis: The many faces of HIF, 254 (2) (2008) 508–513.

[20] B. Bedessem, A. Stéphanou, A mathematical model of HiF-1α-mediated response to hypoxia on the G1/S transition, 248 (2014) 31–39.
[21] B. Zhang, H. Ye, A. Yang, Mathematical modelling of interacting mechanisms for hypoxia mediated cell cycle commitment for mesenchymal stromal cells, BMC Syst. Biol. 12 (2018) 35.
[22] A. Coulibaly, A. Bettendorf, E. Kostina, A.S. Figueiredo, S.Y. Velasquez Giraldo, H.-G. Bock, M. Thiel, H.A. Lindner, M.V. Barbarossa, Interleukin-15 signaling in HIF-1α regulation in natural killer cells, insights through mathematical models, Front. Immunol. 10 (1) (2019) 2401.
[23] S. Taneja, S.W. Vetter, E. Leclerc, Hypoxia and the receptor for advanced glycation end products (RAGE) signaling in cancer, Int. J. Mol. Sci. 22 (15) (2021) 8153.
[24] E. Berra, E. Benizri, A. Ginouvès, V. Volmat, D. Roux, J. Pouysségur, HIF prolyl-hydroxylase 2 is the key oxygen sensor setting low steady-state levels of HIF-1α in normoxia, EMBO J. 22 (16) (2003) 4082–4090.
[25] R.J. Appelhoff, Y.-M. Tian, R.R. Raval, H. Turley, A.L. Harris, C.W. Pugh, P.J. Ratcliffe, J.M. Gleadle, Differential function of the prolyl hydroxylases PHD1, PHD2, and PHD3 in the regulation of hypoxia-inducible factor, J. Biol. Chem. 279 (37) (2004) 38458–38465.
[26] E. Metzen, U. Berchner-Pfannschmidt, P. Stengel, J. Marxsen, I. Stolze, M. Klinger, W.Q. Huang, C. Wotzlaw, T. Hellwig-Burgel, W. Jelkmann, H. Acker, J. Fandreyothers, Intracellular localisation of human HIF-1α hydroxylases: implications for oxygen sensing, J. Cell Sci. 116 (7) (2003) 1319–1326.
[27] M. Jaśkiewicz, A. Moszyńska, J. Króliczewski, A. Cabaj, S. Bartoszewska, A. Charzyńska, M. Gebert, M. Dabrowski, J.F. Collawn, R. Bartoszewski, The transition from HIF-1 to HIF-2 during prolonged hypoxia results from reactivation of PHDs and HIF1A mRNA instability, 2022, Preprint.
[28] J. Korbecki, D. Simińska, M. Gassowska-Dobrowolska, J. Listos, I. Gutowska, D. Chlubek, I. Baranowska-Bosiacka, Chronic and cycling hypoxia: Drivers of cancer chronic inflammation through HIF-1 and NF-κb activation: A review of the molecular mechanisms, Int. J. Molec. Sci. 22 (19) (2021) 10701.
[29] S. Tay, J.J. Hughey, T.K. Lee, T. Lipniacki, S.R. Quake, M.W. Covert, Single-cell NF-κB dynamics reveal digital activation and analogue information processing, Nature 466 (7303) (2010) 267–271.
[30] D. Ehrismann, E. Flashman, D.N. Genn, N. Mathioudakis, K.S. Hewitson, P.J. Ratcliffe, C.J. Schofield, Studies on the activity of the hypoxia-inducible-factor hydroxylases using an oxygen consumption assay, Biochem. J. 401 (1) (2007) 227–234.
[31] S. Pektas, M.J. Knapp, Substrate preference of the HIF-prolyl hydroxylase-2 (PHD2) and substrate-induced conformational change, J. Inorg. Biochem. 126 (2013) 55–60.
[32] P. Koivunen, M. Hirsila, Kari I. K., J. Myllyharju, The length of peptide substrates has a marked effect on hydroxylation by the hypoxia-inducible factor prolyl 4-hydroxylases, J. Biol. Chem. 281 (39) (2006) 28712–28720.
[33] W.G. Kaelin, P.J. Ratcliffe, Oxygen sensing by metazoans: the central role of the HIF hydroxylase pathway, Molec. Cell 30 (4) (2008) 393–402.
[34] J.R. Tuckerman, Y. Zhao, K. S Hewitson, Y.-M. Tian, C.W. Pugh, P.J. Ratcliffe, D.R. Mole, Determination and comparison of specific activity of the HIF-prolyl hydroxylases, FEBS Lett. 576 (1–2) (2004) 145–150.
[35] B.-H. Jiang, G.L. Semenza, C. Bauer, H.H. Marti, Hypoxia-inducible factor 1 levels vary exponentially over a physiologically relevant range of O2 tension, Am. J.Physiol. - Cell Physiol. 271 (4) (1996) C1172–C1180.
[36] L. Holmquist-Mengelbier, E. Fredlund, T. Löfstedt, R. Noguera, S. Navarro, H. Nilsson, A. Pietras, J. Vallon-Christersson, Å. Borg, K. Gradin, L. Poellinger, S. Pahlman, Recruitment of HIF-1α and HIF-2α to common target genes is differentially regulated in neuroblastoma: HIF-2α promotes an aggressive phenotype, Cancer Cell 10 (5) (2006) 413–423.
[37] P. Ferrante, L. Preziosi, Modelling HIF-PHD dynamics, Math. Models Comput. Simul. Biomed. Appl. (2022).
[38] Moreno R.E., A. Yaromina, R. Houben, A.J. Groot, L. Dubois, M. Vooijs, Prognostic role of hypoxia-inducible factor-2α tumor cell expression in cancer patients: A meta-analysis, Front. Oncol. 8 (2018) 224.
[39] L. Chen, Y. Shi, J. Yuan, Y. Han, R. Qin, Q. Wu, B. Jia, B. Wei, L. Wei, G. Dai, HIF-1 alpha overexpression correlates with poor overall survival and disease-free survival in gastric cancer patients post-gastrectomy, PLoS One 9 (3) (2014) e90678.
[40] G.L. Semenza, Pharmacologic targeting of hypoxia-inducible factors, Ann. Rev. Pharm. Toxic. 59 (2019) 379–403.
[41] M. Tafani, B. Pucci, A. Russo, L. Schito, L. Pellegrini, G.A. Perrone, L. Villanova, L. Salvatori, L. Ravenna, E. Petrangeli, M.A. Russo, Modulators of HIF1α and NFkB in cancer treatment: is it a rational approach for controlling malignant progression? Front. Pharm. 4 (2013) 13.
[42] T. Yu, B. Tang, X. Sun, Development of inhibitors targeting hypoxia-inducible factor 1 and 2 for cancer therapy, Yonsei Med. J. 58 (3) (2017) 489–496.
[43] D.P. Stiehl, R. Wirthner, J. Koditz, P. Spielmann, G. Camenisch, R.H. Wenger, Increased prolyl 4-hydroxylase domain proteins compensate for decreased oxygen levels: evidence for an autoregulatory oxygen-sensing system, J. Biol. Chem. 281 (33) (2006) 23482–23491.
[44] M.Y. Koh, G. Powis, Passing the baton: the HIF switch, Trends Biochem. Sci. 37 (9) (2012) 364–372.
[45] S.R. McKeown, Defining normoxia, physoxia and hypoxia in tumours-implications for treatment response, Brit. J. Radiol. 87 (1035) (2014) 20130676.
[46] M. Hirsila, P. Koivunen, V. Gunzler, K.I. Kivirikko, J. Myllyharju, Characterization of the human prolyl 4-hydroxylases that modify the hypoxia-inducible factor, J. Biol. Chem. 278 (33) (2003) 30772–30780.
[47] F.R. Lorenzo, C. Huff, M. Myllymäki, B. Olenchock, S. Swierczek, T. Tashi, V. Gordeuk, T. Wuren, G. Ri-Li, D.A. McClain, T.M. Khan, P.A. Koul, P. Guchhait, M.E. Salama, J. Xing, G.L. Semenza, E. Liberzon, A. Wilson, T.S. Simonson, L.B. Jorde, W.G. Kaelin, P. Koivunen, J.T. Prchal, A genetic mechanism for Tibetan high-altitude adaptation, Nature Genet. 46 (9) (2014) 951–956.
[48] W.G. He, S. Batty-Stuart, J.E. Lee, M. Ohh, HIF-1α hydroxyprolines modulate oxygen-dependent protein stability via single VHL interface with comparable effect on ubiquitination rate, J. Molec. Biol. 433 (22) (2021) 167244.